PERGAMON

Progress in Energy and Combustion Science 27 (2001) 523–545

PROGRESS IN ENERGY AND COMBUSTION SCIENCE

www.elsevier.com/locate/pecs

Nonequilibrium in the transport of heat and reactants in combustion in porous media

A.A.M. Oliveira[1], M. Kaviany*

Department of Mechanical Engineering and Applied Mechanics, University of Michigan, 2350 Hayward Avenue, 2250 G.G. Brown Laboratory, Ann Arbor, MI 48109-2125, USA

Received 17 August 1999; accepted 21 November 2000

Abstract

Combustion in inert, catalytic and combustible porous media occurs under the influence of a large range of geometric length scales, thermophysical and thermochemical properties, and flow, heat and mass transfer conditions. As a result, a large range of phenomenological length and time scales control the extent of departure from local thermal and chemical nonequilibrium. The use of intraphase and interphase nonequilibria have allowed for the design of new combustion processes and systems, such as, catalytic reactors and converters, porous radiant burners, direct energy and gas conversion devices and systems, chemical sensors, and material synthesis processes. Improvement of current and design of yet newer and more innovative systems requires further investigations into the gas-phase and surface chemistry, solid-state and condensed-phase physics, transport in disordered structures, and mathematical and numerical methods. Here we summarize the processes leading to thermal and chemical nonequilibrium, their role in the combustion in porous media, their innovative uses and effects on applications, the current modeling of these processes and the modeling techniques that may allow for further improvements and developments.

Keywords: Combustion; Porous media; Heat transfer; Nonequilibrium; Heterogeneous media

Contents

* Corresponding author. Tel.: +1-734-764-2694; fax: +1-734-647-3170.
E-mail addresses: amirol@emc.ufsc.br (A.A.M. Oliveira), kaviany@umich.edu (M. Kaviany).
[1] Present address: Department of Mechanical Engineering, Federal University of Santa Catarina, CEP 88040-900, Florianópolis, SC, Brazil.

0360-1285/01/$ - see front matter
PII: S0360-1285(00)00030-7

Nomenclature

a	reaction rate constant, m/s
A	area, m^2
A/F	air/fuel mass ratio, kg/kg
A_o	preexponential factor, s^{-1}
$A_{\beta\sigma}$	$\beta\&\sigma$ surface area, m^2
c_p	specific heat capacity, J/(kg K)
d, D	diameter, m
Da	Damköhler number
$D_{i,m}$	molecular mass diffusivity, m^2/s
$D^{\beta}_{i,e}$	effective mass diffusivity, m^2/s
D^{β}_{m}	axial mass dispersion coefficient, m^2/s
D^{β}_{T}	axial thermal dispersion coefficient, m^2/s
D_o	mass diffusion preexponential factor, m^2/s
$f_{\beta\gamma}$	fluid/fluid specific surface area ratio
g_{ψ}	catalytic active surface area ratio
k	molecular thermal conductivity, W/(m K)
$\langle k_e \rangle^{\beta}$	effective thermal conductivity, W/(m K)
l	unit-cell characteristic length, m
L	system-level characteristic length, m
$\dot{m}_i$	mass flux, kg/(m^2 s)
$\dot{\mathbf{m}}_i$	mass flux vector, kg/(m^2 s)
M	molecular weight, kg/kmol
$\dot{n}_{r,i}$	volumetric reaction rate for species i, kg/(m^3 s)
$\dot{n}_{r,j,\beta}$	volumetric reaction rate for reaction j, kmol/(m^3 s)
$\dot{n}_{r,j,\beta\sigma}$	surface reaction rate for reaction j, kmol/(m^2 s)
N_r	number of reactions
Nu_{β}	Nusselt number
$\mathbf{n}_{\beta\sigma}$	normal unit vector
Pe	mass Peclet number
$\mathbf{q}$	heat flux vector, W/m^2
R_g	universal gas constant J/(kmol K)
$\dot{s}$	volumetric thermal energy conversion, W/m^3
$\dot{S}$	energy conversion rate, W
Sh_{β}	Sherwood number
$S_{\beta\sigma}$	specific surface area, m^2/m^3
t	time, s
T	temperature, K
u	velocity, m/s
$\mathbf{u}$	velocity vector, m/s
V	volume, m^3
x	position, m

Greek symbols

δ	thickness, m
ΔE_d	diffusion activation energy, J/kmol
$\Delta h_{r,l}$	heat of reaction, J/kg
ε	porosity
ϕ	stoichiometric ratio, Thiele modulus
ν	number of moles, kmol
ρ	mass concentration, density, kg/m^3

Subscripts and superscripts

a, ad	adiabatic
e	effective
ex	excess
f	fuel
F	flame or front
g	gas
i	species i
j	reaction j
k	conduction
ku	surface convection
l	representative elementary volume
L	system-level
m	mass, mixture
n	nonreacted
o	oxidizer
P	product
r	radiation, reaction, reacted
R	reactants
s	stoichiometric
T	thermal
u	convection
β	phase β

Other symbols

$\langle\ \rangle$	local volume-averaged
$\langle\ \rangle^{\beta}$	local phase-volume-averaged

1. Introduction

Porous media may present a large range of pore sizes, porosities, pore connectivity, and specific interfacial areas between phases. The solid phase may range from organic to ceramic and metallic and the fluid phases may have properties ranging from low-pressure gases to liquid macromolecules. This combination of a variety of length scales and physical properties allows for large thermal, chemical, and mechanical nonequilibria among and within phases. We can define nonequilibria with the help of Fig. 1, which presents a rendering of a porous medium characterized by three levels of geometric length scales, the system level L, the pellet level D and the catalytic surface level d, i.e. a multiple-length scales porous medium. Local thermal nonequilibrium at a given length scale, say the length scale characterized by the dimension D in Fig. 1, by definition, occurs when the difference among the local temperature of the phases is comparable in magnitude to the temperature difference across the length scale immediately larger, e.g. the macroscopic temperature difference across the medium length scale L. This results in local heat transfer among phases which can be sustained through the intraphasic heat transfer or heat generation/consumption. Local chemical nonequilibrium occurs when the difference among the species chemical potential in the phases is comparable in magnitude

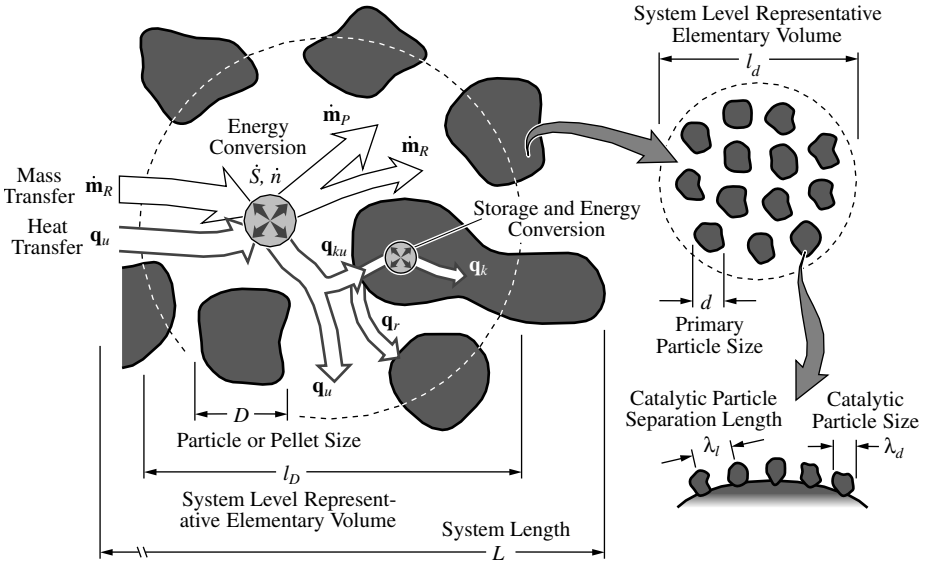

Fig. 1. Rendering of a porous medium formed by a continuous gas phase and a dispersed solid phase showing the different length scales and the heat and mass transfer processes that may take place in the gas and solid phases.

to the differences across the length scale immediately larger. This results in mass transfer across the interfaces which can be sustained through the intraphase mass transport and chemical reaction. Mechanical nonequilibrium occurs when there are variations in fluid phase pressures comparable in magnitude to the differences across the length scale immediately larger, or as a result of a nonzero force balance at solid surfaces. This results in fluid flow and movement of the solid matrix. The transport and kinetic resistances may delay or prevent the system of reaching equilibrium within the residence times characteristic of the process. These nonequilibria are in contrast to the local thermodynamic equilibrium, which is usually assumed to exist at phase interfaces.

Nonequilibria occur because of intrinsic characteristics of the medium, e.g. nonuniform distribution of reactants, noncontinuous solid phase, large mismatch between the thermal properties of the fluid and solid phases, or as a consequence of the process to which it is subjected, e.g. fast transients, highly endothermic or exothermic reactions and large variations in the inlet and outlet conditions. The possibility of nonequilibrium allows for redistribution of heat and reactants over large sections of the medium, energy storage and recirculation, enhanced reaction rates and the formation and freezing of metastable solid phases. As an example, Fig. 2 shows the specific surface area requirement for solid-phase catalytic reactions [129]. High activation energy reactions can occur (the shaded region) if there is a large enough specific surface area. For incomplete covering with active catalytic sites, the required specific surface area increases proportionally.

The use of porous media in combustion systems results in many advantages, but also poses special challenges for the modeling. The volume-averaged models filter out the detailed information at the smaller scales. In most cases, to detect important nonequilibria, one must use detailed local simulations, either using continuum or molecular models, in network or detailed representations of the geometry. Also, in face of the difficulties in obtaining measurements at a pore level, the detailed local simulations have filled in the gaps in the understanding of the physics at the pore level and its interactions with the macroscopic average variables. Examples of the use of average continuum models (e.g. volume-averaged models) and detailed local simulations point out to the need of combining both

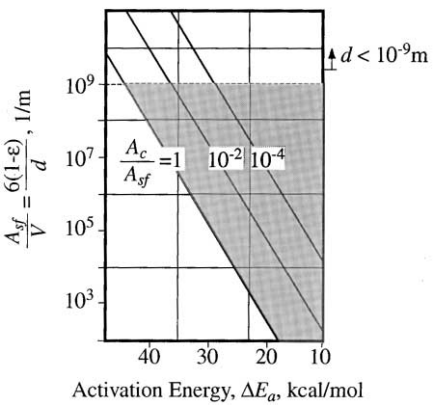

Fig. 2. Specific surface area A_{sf}/V requirement for catalytic solid reaction as a function of the reaction activation energy ΔE_a for different area fractions of active catalytic sites A_c/A_{sf} ($p = 1$ atm, $T = 500$ K, surface concentration $\langle c_i \rangle^s = 0.1$ mol/(cm^2 s), minimum reaction rate $\langle \dot{n}_{r,i} \rangle = 10^{-6}$ mol/(cm^3 s) [129].

modeling strategies in approaching a problem towards the development of new and innovative engineering solutions.

In the following, we review the characteristics of porous media leading to thermal and chemical nonequilibrium, the modeling with volume-averaged continuum equations and the need for detailed local simulations. Examples in which thermal and chemical nonequilibrium is desired or may prevent the obtention of a product or result are presented.

2. Description and modeling

Physically, a porous medium is formed by a solid phase and one or more fluid phases. The solid may have a periodic or random structure, each phase may be continuous or dispersed and the characteristic sizes of the geometric heterogeneities (Fig. 1) may span a large range of length scales. These length scales can either differ by orders of magnitude (i.e. they are separated) or they may vary almost continuously in order of magnitude (i.e. they are continuous). For particulate media, the geometric heterogeneities are the result of large differences in particle sizes and nonuniform distribution and agglomeration of particles with different sizes. For continuous media (e.g. wire meshes, foams, etc.), the heterogeneities are the result of size, aspect ratio and spatial distribution of the solid wires. Chemically, the solid phase may be either inert or it may participate directly in the reactions as a catalytic surface or a source of fuel. Fig. 1 also represents the different heat (the intraphase convection $\mathbf{q}_u$, conduction $\mathbf{q}_k$ and radiation $\mathbf{q}_r$, and the interphase surface convection $\mathbf{q}_{ku}$) and mass (generically shown as reactants $\dot{\mathbf{m}}_R$ and products $\dot{\mathbf{m}}_P$) flux vectors, and the energy and mass conversion and storage (energy conversion $\dot{S}$, mass conversion $\dot{n}$) that are used to describe the transport and reaction during combustion in porous media. For inert or catalytic media, the geometric characteristics result from the manufacturing, and for combustible media, they appear as a consequence of the combustion process (e.g. solid combustion, phase change, phase crystallization, growth and coalescence, etc.). Finally, the phases may be permanently continuous or may change with the reaction, as in the poisoning by pore blockage of catalytic surfaces, and a percolation threshold may be reached in which the transport of heat or mass along a phase is interrupted.

All the physical and chemical processes have phenomenological length and time scales, such as flame thickness, penetration depth, residence time, etc. The phenomenological length scales can be of the same order of magnitude or much different from the geometric length scales. The interaction among the different phenomenological length and time scales and the geometric scales, results in different transport and reaction regimes and leads to thermal and chemical nonequilibria. Fig. 3 shows different examples of pore-level and system-level chemical nonequilibrium. They are classified accordingly to the distribution and to the physical process controlling the mixing of reactants. Fig. 3a is characteristic of the combustion of premixed gas mixtures inside a porous medium, as in the porous burners [1–17,46,47,94–96], catalytic converters [18–21] and combustors [22–37], and energy regeneration devices [38–45]. The solid phase may be either chemically inert or catalytic and both homogeneous and heterogeneous reactions may take place. The flow of reactants and products may be either pressure or diffusion driven. Only the last scale with a nonporous solid phase is represented. In Fig. 3b a porous burner for which the fuel supply is nonuniform is depicted. This is useful in controlling the amount of heat generated per unit volume (or area) of the porous burner either to satisfy the demand for heat (the heat is radiated out from the burner surface) [46,47] or to control the maximum temperature in the burner [48]. The flow of reactants is pressure driven and good mixing is usually assumed. Fig. 3c presents the case in which the fuel is provided from the pyrolysis of the solid, as in solid combustion or smoldering [52–58] and particulate trap regeneration [59–61], or from evaporation of liquid in the form of droplets [49–51]. In this case, the rate of pyrolysis or evaporation may control the reaction. The reaction could also occur inside the solid phase (not depicted) and controlled by the transport of oxidizer or products. Fig. 3d shows an example in which both the reactants come from the solid particles (of different materials), with the reaction occurring in the gas phase. This may be the case of some solid- and condensed-phase combustion synthesis [65,66]. The reactants mixing may be controlled by the rates of generation or by mass transfer. The product in the liquid or gas phase can then nucleate and crystallize as a solid product. Finally, Fig. 3e shows the reaction occurring inside one of the reactant particles, as in gasless combustion synthesis [62–69]. The reactants mixing are controlled by the transport in the pore space (by diffusion or capillarity) and within the reactant B particle (by diffusion). The product may be in the solid phase, growing around the reactant B particle, or in the liquid phase, later nucleating and growing as a solid phase. These mixing effects depicted in Fig. 3a–e can be manipulated to some extent. For example, the control of the distribution of fuel in a porous burner leads to distributed heating [46,47]. In another example, the maximization of reactant mixing in combustion synthesis by controlling the particle size and particle size distribution leads to higher conversion rates [67,68]. To better control the geometry of the medium and the processes occurring there, a fundamental understanding of the interaction among the various processes and scales is needed.

2.1. Modeling

When the scales are sufficiently separated, the use of continuum (or volume-averaged, or homogeneous) models is common. Otherwise, when there is an almost continuous variation of length scales, detailed local simulation is needed.

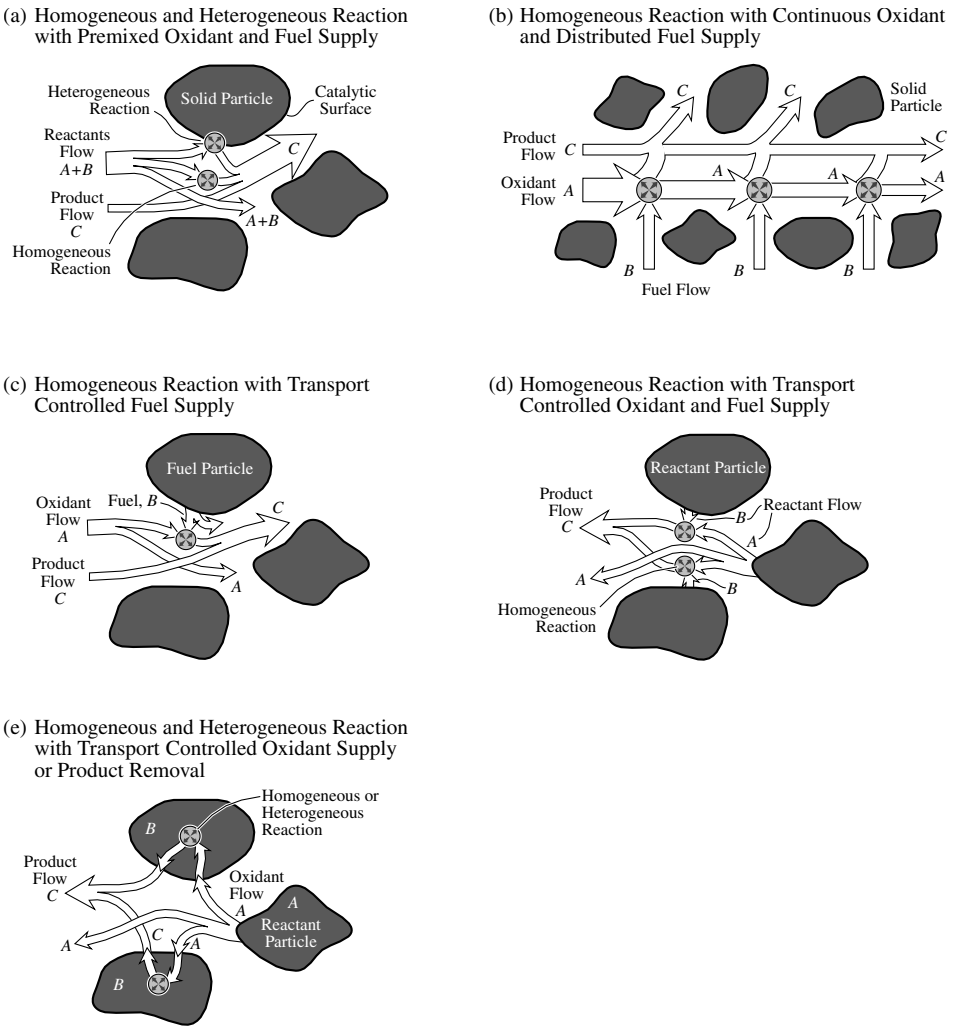

Fig. 3. Distribution and transport of reactants in chemical nonequilibrium processes.

The volume-averaged models are obtained from the averaging of the point-wise conservation equations, starting with two phases β and σ in contact and for which the continuum hypothesis and the thermodynamic equilibrium at phase interfaces hold [123]. Rigorous derivations of volume-averaged conservation equations are available when the phase interfaces are stationary, for binary mixtures and in the absence of cross effects [70,74,78]. The intrinsic phase-average of a scalar or vector quantity ϕ_β is defined as the volume average of that quantity for phase β over the volume V_β occupied by phase β inside an elementary representative volume, $V = V_\beta + V_\sigma$, i.e.

$$\langle \phi_\beta \rangle^\beta \equiv \frac{1}{V_\beta} \int_{V_\beta} \phi_\beta \, \mathrm{d}V = \frac{1}{\varepsilon_\beta} \left(\frac{1}{V} \int_{V_\beta} \phi_\beta \, \mathrm{d}V \right) \equiv \frac{1}{\varepsilon_\beta} \langle \phi_\beta \rangle \tag{1}$$

where $\varepsilon_\beta = V_\beta / V$ is the volume fraction occupied by phase β. The choice of the size of the elementary representative volume V is such that it is large compared to the pore- (or particle-) level geometric length scale but small compared to the system-level geometric length scale. At the same time, it must be smaller than both the pore- and system-level phenomenological length scales. Naming l the characteristic dimension of the representative elementary volume, these conditions can be expressed in their simplest forms as

$$d \ll l \ll L, \qquad l \ll \delta_{i,\mathrm{l}} \text{ and } l \ll \delta_{i,\mathrm{L}} \tag{2}$$

where δ_i are the different phenomenological length scales at the l and L geometric scales. For example, for a catalytic reaction inside a porous radiant burner, l should be smaller than the mass boundary layer thickness $\delta_{\mathrm{y,l}}$, to be able to capture the bulk rate of conversion of reactants. These conditions are met for fully developed flows. However, to capture the entrance effects in high-temperature catalytic burners, l should be smaller than the pore entrance length

$\delta_{x,l}$ and this is usually not met, because the entrance length for the chemically reacting flow is of the order of magnitude of the pore diameter [26,34]. In another example, in combustion synthesis, large concentration gradients, comparable to the system-level concentration gradients, are developed at a particle-level and a single representative elementary volume cannot be defined [67,69]. In general, for those length scales that meet the requirements, we define a representative elementary volume and integrate the equations inside this volume, then filtering out any process occurring at the smaller scales.

The volume-averaged equations require relations for the fluxes at phase interfaces and closure relations for averages of fluctuations. An assumption used to arrive at the closure relations is the linear relation between fluctuations and the gradient or difference of average quantities (e.g. [78,133]). The linear approximation is strictly valid only for small variations of the field of fluctuations when compared to the variations of the averaged values and for short relaxation times at the local scale. As we have seen above, this may not be true, depending on the importance of entrance lengths and boundary layer thicknesses. In order to arrive at closure relations for these situations, we would need higher order expansions for the field of fluctuations, with increasingly higher mathematical difficulty. An alternative to bypass this difficulty is to attempt a solution for the particle- and pore-level problem and then pass the results on to the volume-averaged equations through the interfacial flux terms (source terms). The solution for the local problem can rely on a simpler set of boundary conditions when there is sufficient separation of length scales. This is the nature of shrinking-core models for reactions in beds of catalytic particles, nonequilibrium models for reactive distillation [130,131], small-droplet evaporation models for spray or particle combustion [125,126] and combustion synthesis models [67,68]. When there is not sufficient separation, detailed numerical simulation of the entire system-level domain is necessary. This is particularly the case for catalytic reactions in high temperature, short catalytic burners [34–37].

In the following, the empirical modeling of catalytic reactions using volume-averaging is presented as an example of modeling of a system with sufficient separation of length scales.

2.2. Volume-averaging treatment

For those problems conveniently characterized by a separation of length scales, two- (and three-) medium treatments are developed to model the nonequilibrium among phases. Examples of systems for which separation of length scales exist are catalytic reactors and converters, combustion of solid fuels (except pulverized), and combustion synthesis. The connection between an equation for a level and the equations for the levels immediately below is done through the source term. The closure of the model will depend whether local equilibria can be assumed for the subsequent levels.

The usual way of arriving at the volume-averaged equations is to begin at the innermost scale and move up to the outer scales by a process of upscaling. Here, because the emphasis is on the modeling of nonequilibrium, we will take the opposite direction. In the first level of complexity, the system is formed by two homogeneous phases β and σ. The equation for the conservation of a chemical species i in the β phase has been commonly written as [70–83,133]

$$\frac{\partial}{\partial t}\varepsilon_\beta\langle\rho_i\rangle^\beta + \nabla\cdot\left[\langle\rho_i\rangle^\beta\langle\mathbf{u}_\beta\rangle - \varepsilon_\beta\langle\rho\rangle^\beta(D^\beta_{i,\mathrm{e}} + D^\beta_{\mathrm{m}})\nabla\frac{\langle\rho_i\rangle^\beta}{\langle\rho\rangle^\beta}\right] = \varepsilon_\beta\langle\dot{n}_{\mathrm{r},i}\rangle^\beta \tag{3}$$

where $D^\beta_{i,\mathrm{e}}$ is the effective multicomponent diffusivity of species i in the mixture, D^β_{m} the mass dispersion coefficient and $\langle\dot{n}_{\mathrm{r},i}\rangle^\beta$ the volume-averaged reaction rate. Allowing for both homogeneous in the bulk β phase $\langle\dot{n}_{\mathrm{r},i}\rangle^\beta_\beta$ and heterogeneous at the βσ interface $\langle\dot{n}_{\mathrm{r},i}\rangle^\beta_{\beta\sigma}$ reactions, the intrinsic phase averaged reaction rate for phase β can be modeled as

$$\langle\dot{n}_{\mathrm{r},i}\rangle^\beta = \langle\dot{n}_{\mathrm{r},i}\rangle^\beta_\beta + \langle\dot{n}_{\mathrm{r},i}\rangle^\beta_{\beta\sigma} \tag{4}$$

where $\langle\dot{n}_{\mathrm{r},i}\rangle^\beta_\beta$ depends on the kinetic of the homogeneous reactions,

$$\langle\dot{n}_{\mathrm{r},i}\rangle^\beta_\beta = \left\langle M_i\sum_{j=1}^{N_\mathrm{r}}\nu_{i,j,\beta}\dot{n}_{\mathrm{r},j,\beta}\right\rangle^\beta \simeq M_i\sum_{j=1}^{N_\mathrm{r}}\nu_{i,j,\beta}\dot{n}_{\mathrm{r},j,\beta}(\langle\rho_i\rangle^\beta,\langle T_\beta\rangle^\beta) \tag{5}$$

and, by defining $\langle\phi_i\rangle^{\beta\sigma}$ as the area-average of ϕ_i on the βσ interface and using $S_{\beta\sigma} = A_{\beta\sigma}/V$ for the specific surface area of the βσ interface, $\langle\dot{n}_{\mathrm{r},i}\rangle^\beta_{\beta\sigma}$ is given by

$$\langle\dot{n}_{\mathrm{r},i}\rangle^\beta_{\beta\sigma} = \langle\dot{m}_i\rangle^{\beta\sigma}\frac{S_{\beta\sigma}}{\varepsilon_\beta} \tag{6}$$

The use of the average temperature and concentrations to evaluate the homogeneous reaction rates in Eq. (5) is an approximation valid for small departures from equilibrium [8].

The βσ interfacial jump condition, at the β side, has been usually modeled as

$$\langle\dot{m}_i\rangle^{\beta\sigma} = -\frac{Sh_\beta D^\beta_{i,\mathrm{m}}}{D_\beta}(\langle\rho_i\rangle^\beta - \langle\rho_i\rangle^{\beta\sigma}) \tag{7}$$

where Sh_β is the interfacial average Sherwood number based on the surface characteristic dimension D_β, $D^\beta_{i,\mathrm{m}}$ the multicomponent diffusivity of species i in the mixture m, and $\langle\rho_i\rangle^{\beta\sigma}$ the concentration of i at the βσ interface.

The σ side of the jump condition, depends on the geometry of phase σ. When phase σ is a plain surface (in contrast to being porous), the jump condition at the σ side results in

$$\langle\dot{m}_i\rangle^{\beta\sigma} = \langle\dot{n}_{\mathrm{r},i}\rangle^{\beta\sigma} \simeq M_i\sum_{j=1}^{N_\mathrm{r}}\nu_{i,j,\beta\sigma}\dot{n}_{\mathrm{r},j,\beta\sigma}(\langle\rho_i\rangle^{\beta\sigma},\langle T_\sigma\rangle^\sigma) \tag{8}$$

where $\dot{n}_{r,j,\beta\sigma}$ is the molar reaction rate for surface reaction j (per unit area of surface) and $\nu_{i,j,\beta\sigma}$ the stoichiometric coefficient of component i in reaction j (with $\nu_{i,j,}\beta\sigma > 0$ when i is a reactant). The use of the solid average temperature to evaluate the surface reaction rate will be discussed with the thermal nonequilibrium.

Eqs. (5)–(8) apply to a porous medium with a plain solid catalytic material, like a pure platinum surface. The surface reaction rate would then be the surface averaged reaction rate for the platinum surface, taking into account the surface characteristics, like orientation of the crystalline planes, poisoning, etc. The use of dispersion coefficients and interphase mass transfer equations like Eq. (7) relies on the kind of linear constitutive relations discussed above. These have been extended to more general situations through the *empirical modeling* of the dispersion and interfacial transfer coefficients. The derivation of the volume-averaged equations shows the correct form and limitations in the use of interfacial flux equations, dispersion fluxes and effective properties.

In the second level of complexity, phase σ may also be porous, having a fluid phase γ and a solid phase ψ, and being characterized by smaller characteristic length scales. The problem for this $\gamma\psi$ medium is then solved separately, but in a coupled way, to the $\beta\sigma$ medium. If we assume local chemical equilibrium for the σ phase, we can average the interfacial jump condition for the σ side of the interface, to give

$$\langle \dot{m}_i \rangle^{\beta\sigma} = -[\langle \dot{\mathbf{m}}_i \rangle^{\sigma} \cdot \mathbf{n}_{\beta\sigma}]_{\beta\sigma} \tag{9}$$

where $\mathbf{n}_{\beta\sigma}$ is the normal to the $\beta\sigma$ interface pointing from β to σ, $\langle \dot{\mathbf{m}}_i \rangle^{\sigma}$ the average mass flux vector at the σ phase,

$$\langle \dot{\mathbf{m}}_i \rangle^{\sigma} = \langle \rho_i \rangle^{\sigma} \langle \mathbf{u}_{\sigma} \rangle - \varepsilon_{\sigma} \langle \rho \rangle^{\sigma} (D^{\sigma}_{i,e} + D^{\sigma}_{m}) \nabla \frac{\langle \rho_i \rangle^{\sigma}}{\langle \rho \rangle^{\sigma}} \tag{10}$$

and in Eq. (7) the concentration of i at the $\beta\sigma$ interface is now given by $\langle \rho_i \rangle^{\beta\sigma} = [\langle \rho_i \rangle^{\sigma}]_{\beta\sigma}$. Note that $\varepsilon_{\beta} + \varepsilon_{\sigma} = 1$.To solve for $\langle \rho_i \rangle^{\sigma}$ a transport equation for the bulk σ phase similar to Eq. (3) is needed,

$$\frac{\partial}{\partial t} \varepsilon_{\sigma} \langle \rho_i \rangle^{\sigma} + \nabla \cdot \langle \dot{\mathbf{m}}_i \rangle^{\sigma} = \varepsilon_{\sigma} \langle \dot{n}_{r,i} \rangle^{\sigma} \tag{11}$$

The volume-averaged reaction rate is also given by

$$\langle \dot{n}_{r,i} \rangle^{\sigma} = \langle \dot{n}_{r,i} \rangle^{\sigma}_{\gamma} + \langle \dot{n}_{r,i} \rangle^{\sigma}_{\gamma\psi} \tag{12}$$

where $\langle \dot{n}_{r,i} \rangle^{\sigma}_{\gamma}$ and $\langle \dot{n}_{r,i} \rangle^{\sigma}_{\gamma\psi}$ are, respectively, homogeneous and heterogeneous reaction rates. When local chemical equilibrium in phase σ is assumed, we have $\langle \rho_i \rangle^{\gamma\psi} = \langle \rho_i \rangle^{\gamma} = \langle \rho_i \rangle^{\sigma}$, and these become

$$\langle \dot{n}_{r,i} \rangle^{\sigma}_{\gamma} = \langle \dot{n}_{r,i} \rangle^{\gamma} \varepsilon_{\gamma,\sigma} \tag{13}$$

$$\langle \dot{n}_{r,i} \rangle^{\sigma}_{\gamma\psi} = \langle \dot{n}_{r,i} \rangle^{\gamma\psi} S_{\gamma\psi,\sigma} \tag{14}$$

where $\langle \dot{n}_{r,i} \rangle^{\gamma}$ and $\langle \dot{n}_{r,i} \rangle^{\gamma\psi}$ are given by equations similar to Eqs. (5) and (8). Note that $\varepsilon_{\gamma,\sigma} + \varepsilon_{\psi,\sigma} = 1$ and $S_{\gamma\psi,\sigma} = A_{\gamma\psi}/V_{\sigma}$.

In the absence of local chemical equilibrium for phase σ, we need to write equations for phase γ similar to the equations used above for phase β. Also, interfacial mass fluxes then occur across the various areas available for flow (micro channels) and heterogeneous reactions may occur at the exposed solid surfaces. An initial difficulty is the definition of the interface position, especially, where the interface should be located at the pore openings, where the fluid phase is in fact continuous. Depending on how deep the interface penetrates into the pores, a larger part of the surface solid area will be in direct contact with the β phase. Also, there could exist locally strong and recirculating convection flows. The transition between a porous and a plain medium was discussed elsewhere, in the context of convection and diffusion [73,83]. Here, we will assume that we can define an interfacial region as a sharp interface (in a way, similar to the Gibbs model for interfaces). Assuming no interaction among the fluxes leaving the $\beta\gamma$ and the $\beta\psi$ interfaces, for a porous phase σ the interfacial mass transfer can be written as

$$\langle \dot{m}_i \rangle^{\beta\sigma} = f_{\beta\gamma} \langle \dot{m}_i \rangle^{\beta\gamma} + (1 - f_{\beta\gamma}) g_{\psi} \langle \dot{m}_i \rangle^{\beta\psi} \tag{15}$$

where $f_{\beta\gamma} = S_{\beta\gamma}/S_{\beta\sigma}$ and $g_{\psi} = A_c/A_{\beta\psi}$ is the apparent fraction of the $\beta\psi$ interface covered by catalytic sites. The equation for $\langle \dot{m}_i \rangle^{\beta\gamma}$ is given by an equation similar to Eq. (9) and for $\langle \dot{m}_i \rangle^{\beta\psi}$, assuming local chemical equilibrium, an equation like Eq. (8) would hold.

In the third level of complexity, phase ψ may also be porous, being formed by a fluid phase δ and a solid phase ω, and the interfacial mass transfer is then written as

$$\begin{aligned} \langle \dot{m}_i \rangle^{\beta\sigma} = {} & f_{\beta\gamma} \langle \dot{m}_i \rangle^{\beta\gamma} + (1 - f_{\beta\gamma})[f_{\beta\delta} \langle \dot{m}_i \rangle^{\beta\delta} \\ & + (1 - f_{\beta\delta}) g_{\omega} \langle \dot{m}_i \rangle^{\beta\omega}] \end{aligned} \tag{16}$$

The mass fluxes at the $\beta\gamma$ and $\beta\delta$ interfaces are given by equations similar to Eq. (9) and the mass flux at the solid surface, assuming zero mass transfer resistance at the $\beta\omega$ and N_r surface reactions, would be given by an equation like Eq. (8).

This cascade of fluxes (and levels) is interrupted when all the interfaces and phases inside a region are in thermal and chemical equilibrium. At this last level, thermodynamic equilibrium equations are written for closure. However, the use of a surface average for this last scale may still be necessary. The surface reactions occur at crystallites which may be nonuniformly distributed on the surface of the solid particles. The apparent area fractions g_{ω} and g_{ψ}, which account for the concentration, size and shape of the crystallites ($0 \le g_k < \infty$), remain as empirical parameters. The catalytic sites on the crystallites may also vary in activity. For example, the activity of noble metal crystallites depends on lattice orientation, presence of neighboring sites, interaction with the substrate, poisoning, etc. [106,109]. The sizes of the crystallite heterogeneities form the last geometric length scales of interest here. Fig. 4 shows a

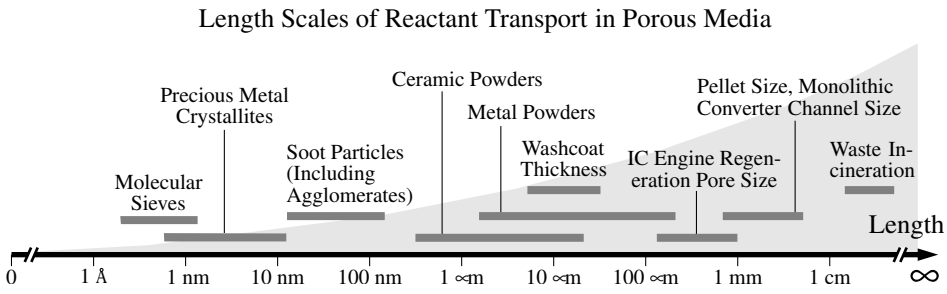

Fig. 4. Length scales and characteristic dimensions for various systems.

summary of these length scales and characteristic dimensions for various systems. The modeling at the smaller scales requires molecular simulation.

The modeling of local thermal nonequilibrium follows in a similar way, using two- and three-medium treatments. Assuming that phase β is transparent to thermal radiation, the thermal energy equation for phase β is commonly written as [83]

$$\frac{\partial}{\partial t}(\varepsilon_\beta\langle\rho c_p\rangle^\beta\langle T_\beta\rangle^\beta) + \nabla\cdot[\langle\rho c_p\rangle^\beta\langle\mathbf{u}_\beta\rangle\langle T_\beta\rangle^\beta - \varepsilon_\beta(\langle k_e\rangle^\beta + \langle\rho_\beta\rangle^\beta c_{p,\beta}D_T^\beta)\nabla\langle T_\beta\rangle^\beta] = \varepsilon_\beta\langle\dot{s}_\beta\rangle^\beta \quad (17)$$

where $\langle k_e\rangle^\beta$ is the effective thermal conductivity and D_T^β is the thermal dispersion coefficient for phase β. One additional difficulty arising when writing these equations is the treatment of the heat source/sink at the phase interfaces. A simpler treatment consists in modeling the volumetric energy generation, in the presence of interfacial heat transfer and homogeneous chemical reaction, as

$$\langle\dot{s}_\beta\rangle^\beta = \frac{S_{\beta\sigma}}{\varepsilon_\beta}\frac{Nu_\beta k_\beta}{D_\beta}(\langle T_\beta\rangle^\beta - \langle T_\sigma\rangle^\sigma) + \sum_{i=1}^{N_c}\langle\dot{n}_{r,i}\rangle_\beta^\beta\Delta h_{r,i} \quad (18)$$

where Nu_β is the interfacial average Nusselt number based on D_β.

Then, for phase σ, assuming it is stationary, we have

$$\frac{\partial}{\partial t}(\varepsilon_\sigma\langle\rho c_p\rangle^\sigma\langle T_\sigma\rangle^\sigma) + \nabla\cdot[-\varepsilon_\sigma(\langle k_e\rangle^\sigma\nabla\langle T_\sigma\rangle^\sigma + \langle q_r\rangle^\sigma)] = \varepsilon_\sigma\langle\dot{s}_\sigma\rangle^\sigma \quad (19)$$

where $\langle q_r\langle^\sigma$ is the radiation heat flux within phase σ. The volumetric energy generation, assuming that there is both homogeneous and heterogeneous chemical reaction at the βσ interface, is

$$\langle\dot{s}_\sigma\rangle^\sigma = -\frac{S_{\beta\sigma}}{\varepsilon_\sigma}\frac{Nu_\beta k_\beta}{D_\beta}(\langle T_\beta\rangle^\beta - \langle T_\sigma\rangle^\sigma) + \sum_{i=1}^{N_c}(\langle\dot{n}_{r,i}\rangle_\sigma^\sigma + \langle\dot{n}_{r,i}\rangle_{\beta\sigma}^\sigma)\Delta h_{r,i} \quad (20)$$

In the model above, as an approximation, it has been assumed that the interfacial region is completely in the σ phase. Under this assumption, the heterogeneous reaction $\langle\dot{n}_{r,i}\rangle_{\beta\sigma}^\sigma$ occurs in the σ phase, causing heating or cooling of the interface, and then there is heat transfer to the β phase by interphase heat transfer. A better model would somehow distribute the heat generated directly into both neighboring phases.

In the following, examples of systems with important thermal and chemical nonequilibrium are given. Then, complementing the volume-averaging modeling of catalytic reactions, the need for detailed simulation is discussed in the context of catalytic reactions in porous media.

3. Thermal nonequilibrium

Intraphase thermal nonequilibrium results in heat transfer by conduction, convection and radiation (volumetric and surface). Interphase thermal nonequilibrium results in heat transfer between phases (surface convection). These inter- and intraphase thermal nonequilibrium, when coupled, are responsible for superadiabatic combustion and thermal regeneration.

3.1. Superadiabatic combustion

Combustion of a gas mixture in the presence of a chemically inert porous medium differs from combustion in a plain medium (i.e. gas phase only) because the thermal properties of the solid and gas phases are vastly different. The thermal conductivity of the solid phase and, as a result, the effective thermal conductivity of the medium, can be several orders of magnitude larger than that of the gas phase. Then, there is an enhanced conduction heat transfer along the solid phase, compared to the gas phase, and surface radiation exchange between particles. The large interfacial surface area between the gas and the solid results in a small resistance for surface-convection heat transfer, i.e. a large local (or pore) value for the number of transfer unit *NTU*. Thus, the heat generated by combustion is readily transferred to the solid phase and locally the surface of the solid phase reaches a temperature close to the gas-phase temperature. As a result, for media which are not optically thick [5,10,89], there is surface radiation heat transfer along the flame. The combined effects of conduction, radiation

and surface convection, cause a substantial preheating of the gas phase. This preheating adds to the energy released by combustion resulting in local temperatures in excess of the adiabatic flame temperature for the gas mixture. This is called superadiabatic combustion and has been applied to increase the burning rates of gas mixtures [1–7,10,94,95] and condensed fuels [50,51], to allow for the combustion of low calorific fuels [4,41], to recuperate energy from reaction processes [42], and to create large thermal gradients in the solid phase [43,44].

The superadiabatic effect is observed for both propagating [94,95] and stabilized flames [4,41]. In a propagating flame, the superadiabatic effect occurs as a result of the overlap of the thermal and the combustion waves [94,95]. The velocity of propagation of a thermal pulse, when there is a gas flow with velocity $\langle u_g \langle$ through the porous media (i.e. the thermal wave speed), is given by

$$u_T = \langle u_g \rangle \frac{\rho_g c_{p,g}}{\langle \rho c_p \rangle}, \tag{21}$$

where $\langle \rho c_p \rangle$ is the volumetric heat capacity of the porous medium (solid phase).

When there is also a combustion wave traveling at the speed u_F, the maximum excess temperature at the combustion wave, assuming an adiabatic medium and a complete combustion of the fuel, is given by Ref. [94]

$$\Delta T_{ex} \equiv T_{ex} - T_n = \Delta T_{ad} \frac{1}{1 - u_F/u_T},$$

where the adiabatic temperature increase is given by

$$\Delta T_{ad} \equiv T_{ad} - T_n = \frac{\rho_f \, \Delta h_{r,f}}{\rho_g c_{p,g}}.$$

For stable propagation, $u_T > u_F$ is required. Note that when $u_F \rightarrow u_T$, i.e. there is a superposition of the two waves, the excess temperature may be very large, even for mixtures with a small heat of reaction $\Delta h_{r,f}$ or for diluted mixtures (small fuel mass concentration ρ_f). For example, a maximum temperature 2.8 times the adiabatic temperature for an air–methane mixture with air/fuel ratio $(A/F)_a = 62$ (stoichiometric ratio $\phi = (A/F)_s/(A/F)_a = 0.28$) has been observed [94]. Note that the flammability limits for methane–air mixtures (1 atm, 300 K) is $9 < (A/F)_a < 27$ $(0.6 < \phi < 1.9)$ [125]. By adjusting the gas flow rate $\langle u_g \rangle$, stable propagation can be achieved over a larger range of air/fuel ratios, $11 < (A/F)_a < 60$ $(0.28 < \phi < 1.6)$.

The heat recirculation also results in the stabilization of the flame in the interior of the porous medium and reduces the susceptibility to extinguishment caused by flow rate fluctuations. There is a range of gas velocity for which the flame is stationary. Reciprocating flow has also been used to create and hold high thermal gradients inside a porous medium at superadiabatic temperatures [4]. This has been used to burn extremely lean mixtures, either in porous burners as well as in combustion engines [41], in converting methane to hydrogen (autothermic reforming) [45] and in direct energy conversion [44]. In these systems, the flame is stabilized in the interior of the medium by periodically reversing the flow. The fuel can be premixed with the oxidizer or direct fuel injection can be used. For example, a direct energy conversion method [44] uses a combustion tube with reciprocating flow and direct fuel injection to create and stabilize a thermal gradient in the solid phase with maximum temperature above the adiabatic flame temperature for the mixture. This gradient is used to power a thermoelectric cell (Peltier effect) and produce electrical energy. Fig. 5 shows a rendering of the combustion tube. The central part of the tube (combustor) is made of an inert material (alumina) and the ends are made of a high-temperature resistant thermoelectric material (e.g. a Si–Ge alloy), as shown in Fig. 5a. Fig. 5b shows the different heat transfer and energy conversion mechanisms. Combustion occurs at the adiabatic region, while thermal to electric energy conversion occurs at the thermoelectric regions. Heat transfer from, at the adiabatic section, and to the gas phase, at the thermoelectric section, occurs by surface convection. Positioning of the fuel injection allows for better control of the flame position. Due to the relatively high thermal conductivity of the combustion section, the exact position of the flame is not critical. Conduction along the thermoelectric section upstream the flame allows for heat recirculation (resulting in superadiabatic effect). However, this also increases the axial heat losses and the conduction heat loss from the hot junction to the cold junction, which reduces the thermoelectric efficiency of the cell. Increasing the length of the thermoelectric section, increases the preheating which leads to higher temperatures and higher thermal efficiency. But, the electrical resistance also increases, resulting in higher Joule heating which leads to smaller thermoelectric efficiency. Therefore, an optimization of the length of the thermoelectric section that maximizes the overall conversion efficiency is possible. For a cylindrical tube 1 mm in diameter, an overall conversion efficiency of 10% has been calculated [44]. By decreasing the thermal conductivity of the thermoelectric material by 70% while keeping the electrical conductivity constant, an efficiency as high as 25% could be achieved. This would make this process competitive when compared to other high efficiency, direct electrical power generation methods.

For porous burners in general, an increase in the specific heat of the medium causes an increase of the temperature gradient. The same effect is achieved when burning richer mixtures. The superadiabatic effect is increased for large radiation extinction coefficients. A small radiation extinction coefficient may lead to extinguishment due to heat transfer with the surroundings. The presence of the porous matrix also affects the pore-level flow and heat transfer. The fluid velocity at the walls is zero and the Taylor–Aris dispersion [83] increases the heat and chemical species diffusion. The reactions are limited to the pore space and the local temperatures may be much higher (200 K [8]) than the volume-averaged gas temperatures. These high local

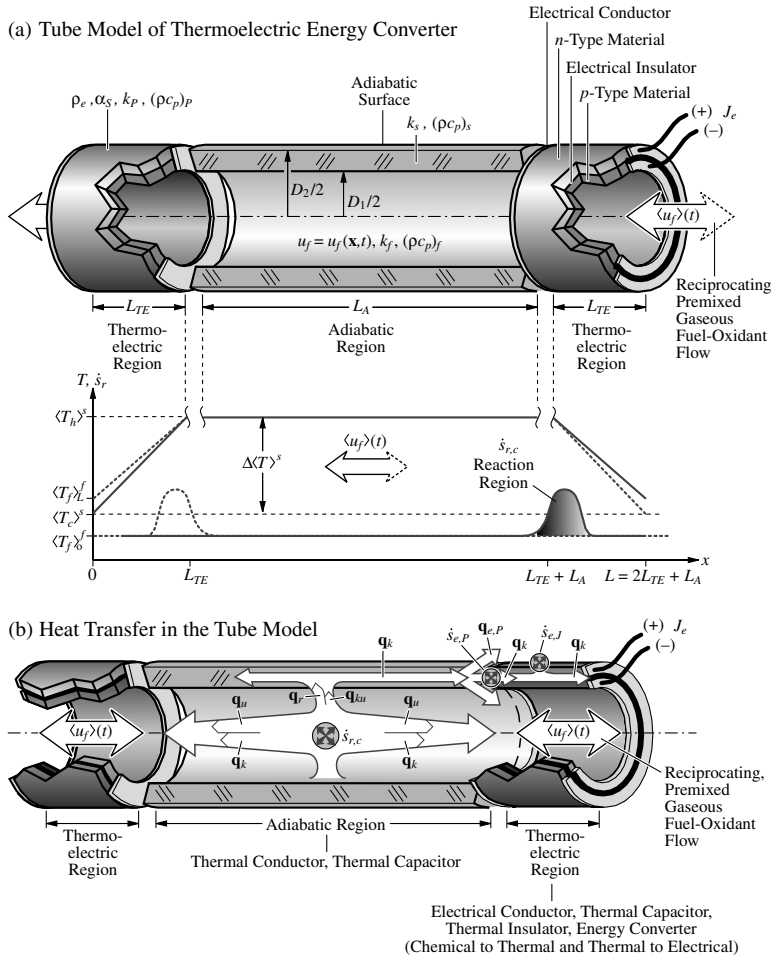

Fig. 5. Rendering of a combustion-thermoelectric tube for electrical energy generation [44].

temperatures may increase the formation of thermal NO_x. The analysis of these effects requires a pore-level solution with multi-step chemistry.

3.2. Radiant porous burners

Radiant porous burners take advantage of superadiabatic stabilized flames and enhanced solid matrix emissivity to radiate heat to an external surface, for example, for infrared heating and drying of surfaces. The efficiency of the radiant burner is proportional to the radiation output [9,10]. This depends on the heat generated by combustion, flame position and the thermal properties of the medium, especially, the radiation properties.

A rendering of the problem is shown in Fig. 6. The premixed gas flowing from the left to the right has the far upstream (nonreacted gas-phase only) conditions of T_n, u_{g_n} and fuel and oxidant densities ρ_{f_n} and ρ_{o_n}. The gas enters into the permeable slab at $x = 0$ and inside the slab the velocity (Darcean velocity) is $\langle u_g \rangle$. The flame may be stabilized at a location x_F and the fluid and solid intraphase heat flow occurs towards the upstream and downstream of the flame. The upstream heating, or preheating, is required for sustaining the reaction and the downstream heat flow occurs to supply the heat loss by radiation from the downstream surface at $x = L$.

Depending on the choice of the solid material and matrix structure, the porous medium can significantly influence the flame speed for the combustion of a gaseous fuel u_F and, as a result, higher combustion rates are possible. This depends on the extent of the radiation and conduction preheating, the interfacial volumetric heat transfer rate, and the downstream radiation heat loss, among other parameters. In addition, for finite porous media, e.g. a permeable slab, the radiation heat loss from the surface of the slab can also influence the flame speed. For optically thick media with high backward scattering [87], the radiant output is maximized when the flame is near the exit of the medium. The reduction of the scattering albedo can be achieved by reducing the size of the fibers [87] and by applying a thin coating over them [9]. For

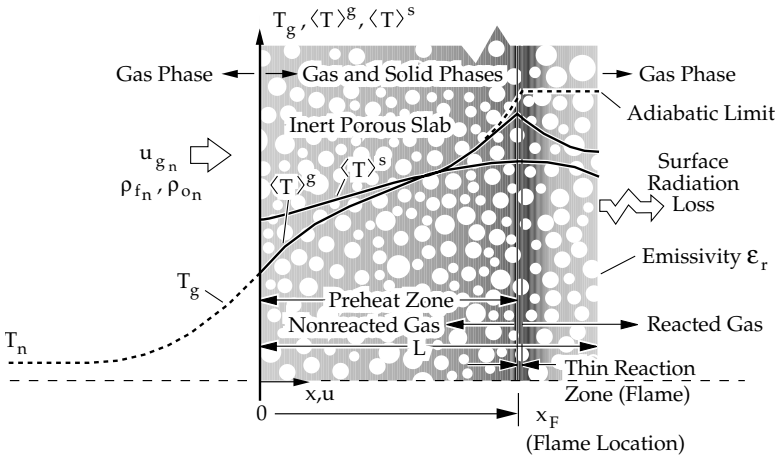

Fig. 6. Rendering of a radiant porous burner showing the solid and fluid temperature distributions (i.e. lack of local thermal equilibrium) for a typical flame location.

different coating materials, there is an optimum coating thickness that maximizes the radiation output. The emissivity of silica fibers with diameter 2.5 μm coated with 6 nm thick platinum or 20 nm thick graphite is increased by a factor of 3 at $T = 1000$ K and 6 at $T = 1500$ K. Silicon oxide may be used to protect the platinum coating against oxidation [9]. During operation, the flame may be placed just outside the permeable slab (or layer), exposing it to the surroundings.

The internal radiation heat transfer can be modeled by considering emission and absorption [5] and by including scattering [3,9,85,87,88,89,90]. For porous burners, the optical thickness τ_r is usually larger than one, and the internal radiation heat transfer is significant [3,9]. The Deissler approximation for the radiant heat flux is appropriate when $\tau_r > 1$. In this case, a radiant conductivity can be used [71–73,75,77,84] to obtain overall efficiency parameters for the porous burner. Thin media or spectral properties require the solution of the radiative transfer equation [9,86,89,90,92] or the use of unit cells [91,93].

Direct local simulation [8] demonstrates the convenience and also the limitation of the volume-averaged treatments and the error expected when the constraints in the applicability of these treatments are not satisfied. The prediction of pollutant formation requires the use of detailed simulation and chemistry. A two-equation model, including dispersion effects on the conservation of energy and species mass equations, may be used for smaller thermal nonequilibrium. For strong thermal nonequilibrium or short burners, direct local simulation may be needed [6,8]. These must be coupled with the appropriate radiation model (e.g. surface radiation exchange).

3.3. Thermal regeneration

A relatively new and innovative idea [38–40] is the use of an in-cylinder porous foam, or porous regenerator, to promote thermal regeneration and catalytic destruction of gaseous and particulate pollutants in diesel engines.

The porous regenerator is attached to a rod and moves up and down inside the cylinder, synchronized to the movement of the piston. Fig. 7 shows a rendering of the cylinder of a diesel engine with the porous regenerator and the position of the piston and porous regenerator along the cycle. For most of the time, the regenerator is close either to the cylinder head or to the top of the piston. During the regenerative cooling stroke, the regenerator moves down, from the cylinder head to the piston top, and during the regenerative heating stroke the regenerator moves up, from the piston top to the cylinder head. Following combustion and expansion, the products of combustion (exhaust gas) still have an appreciable amount of energy in the form of sensible heat. During the regenerative heating stroke, as the regenerator moves up, the hot exhaust gas flowing through it delivers part of its sensible heat to the solid matrix (which has a large specific surface area) by surface-convection heat transfer. This amount of heat is stored as sensible heat. During the regenerative cooling stroke, as the regenerator moves downward, the cold air flowing through it is then heated by the regenerator. Therefore, there is a transfer of heat from the hot exhaust gas to the cold intake air via the regenerator. This principle is also used in the Stirling engines [40,41]. But, in in-cylinder regeneration, the heating of the intake air does not affect the volumetric efficiency of the engine, because heating occurs after the intake air has been admitted to the cylinder. The thermal regeneration depends on the choice of the material and geometry. High solid conductivity, high volumetric heat capacity and low effective thermal conductivity are desirable for optimal heat storage and recirculation. Comparison of the results for the nonregenerative and the regenerative engines using a SiC 12 ppi foam shows that there is a 50%

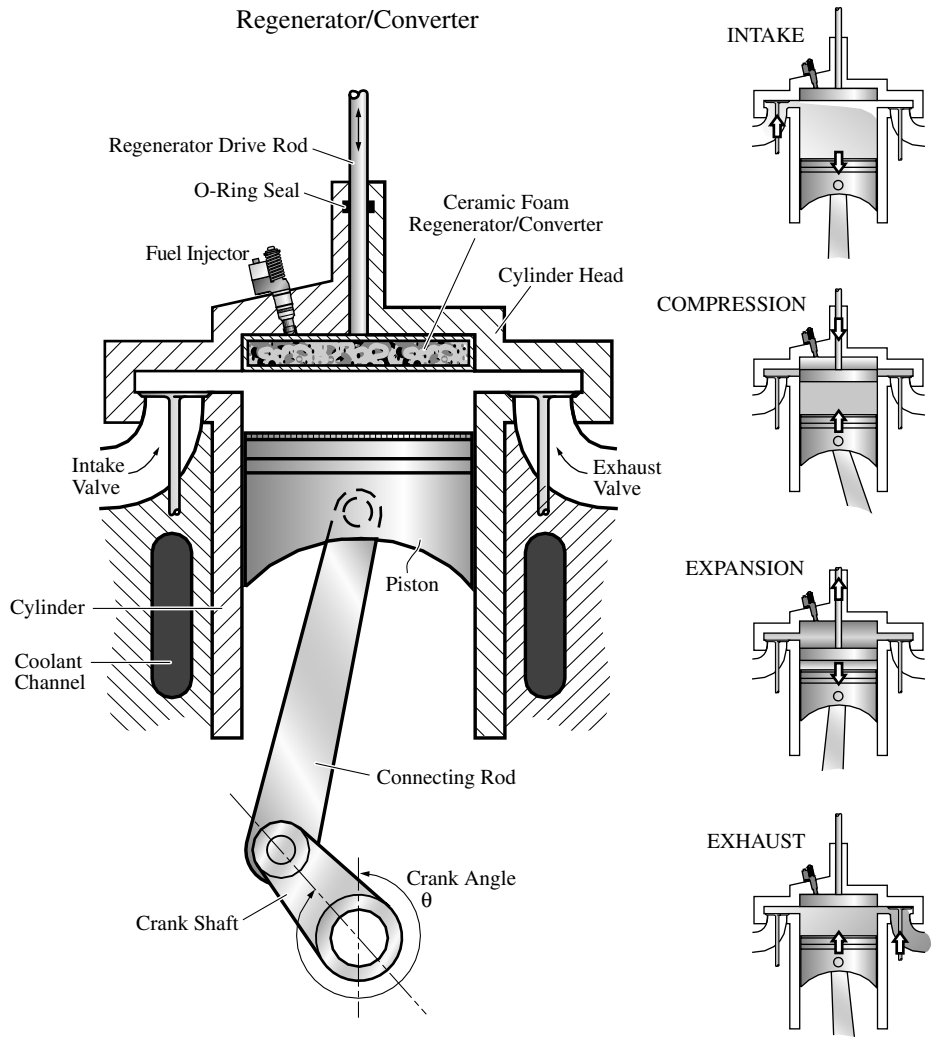

Fig. 7. Rendering of an in-cylinder porous foam for thermal regeneration and catalytic conversion of gas pollutants and particulates in diesel engines, showing the porous regenerator when resting at the top of the combustion chamber and its position during the four-strokes cycle [40].

increase in fuel efficiency and a 33% decrease in specific fuel consumption, for the same air/fuel ratio. There is also an increase in the average gas temperature for the top chamber (where combustion takes place). This high peak temperature is a result of the higher initial temperature of the air (before injection starts) and the smaller amount of air available for combustion. The local higher temperature of the gas in the top chamber may increase the production of thermal NO_x. However, the top–bottom volume-averaged temperature is smaller than the volume-averaged temperature for the nonregenerative engine.

Porous foams can also be used for trapping and combustion of particulates (soot). The porous insert traps part of the soot before it leaves the cylinder and the high temperature reached by the solid phase promotes combustion of the particulates during each cycle.

4. Chemical nonequilibrium

Chemical nonequilibrium may be imposed on the system to control combustion and heat transfer, or it may be a result of the inherent characteristics of the system, e.g. a nonuniform distribution (i.e. mixing) of reactants. Examples of the former are the distributed porous burners, and of the later, are solid pyrolysis and combustion synthesis. In the catalytic converters the geometry is tailored to increase global conversion rates.

4.1. Distributed porous burners

In a conventional nonpremixed and premixed oxygen–methane radiant burner, the combustion is confined to a small region near the fuel inlet, and therefore, only a

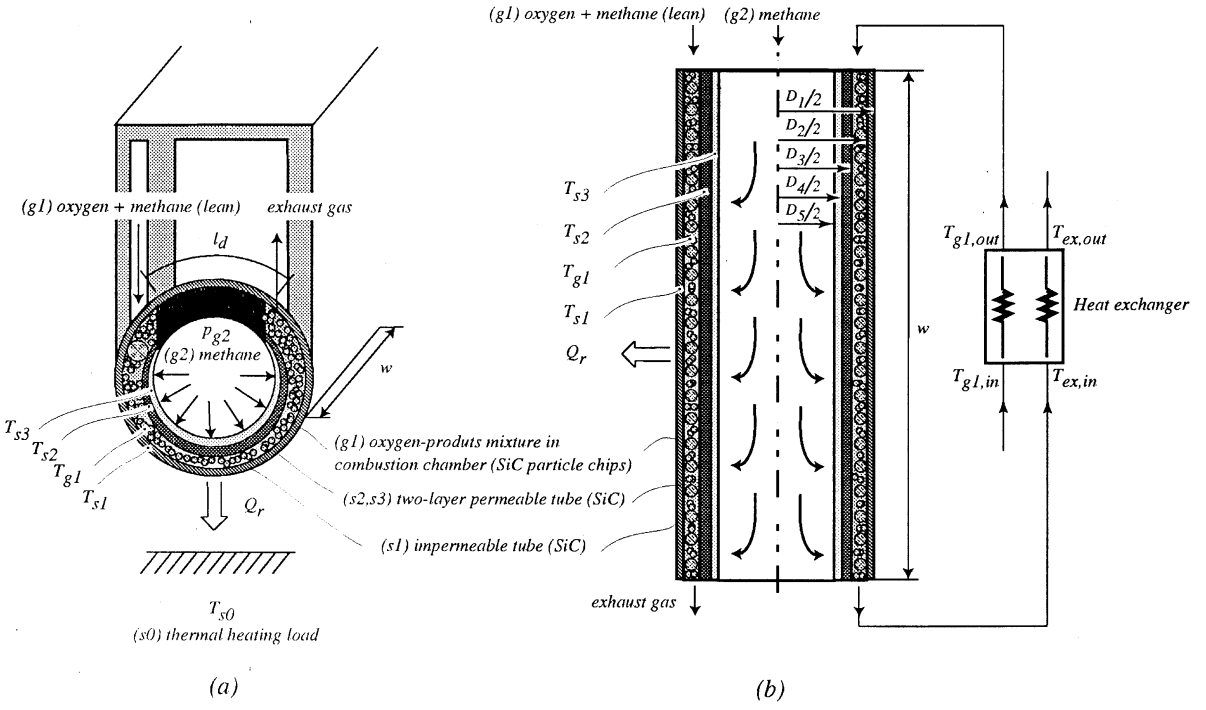

Fig. 8. Rendering of an annular radiant burner showing the (a) transversal and (b) longitudinal cross-sectional views [46,47].

small part of the burner surface contributes to the surface radiation heat delivery. This may result in excessive temperature and meltdown. To reduce the maximum temperature and have a more uniform heating, the fuel should be distributed over the entire volume of the combustion chamber. One method of achieving an optimum distribution of the fuel, is to burn the mixture in an annular combustion chamber with the fuel supplied through a permeable wall, as shown in Fig. 8 [46,47]. Fig. 8a presents a transversal cross-section of the tube showing the fuel and exhaust gas channels, and the annular variable thickness channel (containing particles) in which the combustion occurs. Fig. 8b presents a longitudinal cut of the combustion tube indicating the direction of the methane and exhaust gas flows.

The optimum distribution of fuel is achieved by selecting the proper wall thickness, permeability, and pressure difference between the fuel supply line inside the permeable tube and the combustion chamber. For example, a nonuniform permeable wall thickness results in nonuniform fuel distribution (the flow is pressure driven), creating a nonuniform distribution of reaction rate along the burner which can then be tailored to the distribution of the thermal load. Heat exchange with the exhaust gas (preheating followed by superadiabatic effect) further increases the radiation output and overall burner efficiency. Radiation efficiencies around 90% are possible [46].

The high temperature in the permeable chamber may result in soot formation in the methane (fuel) stream near the inside surface, potentially blocking the fuel passage. To prevent the soot formation, the use of low-conductivity wall materials keeps the temperature of the inside surface of the permeable wall fairly low.

Fuel distribution has also been used to control the maximum temperature for catalytic combustors [48]. The fuel supply can be staged between sections of monolith to keep the adiabatic temperature for the fuel/air mixture below the catalytic surface meltdown temperature.

4.2. Catalytic reactions

Catalytic surfaces are used in catalytic reactors (converters) [18–21] or [21–32] and in complete [21–32] or partial catalytic combustors [33–36]. The catalytic reactors operate at a larger range of temperatures and are designed for improvement in synthesis rates of chemicals, purification and refining, and pollutant destruction. Catalytic combustors are designed for the production of power, heat (by radiation or convection), partial decomposition of heavier compounds, incineration, and regeneration and reforming. The catalytic converters and reactors are typically formed by a catalytic surface attached to a monolith, metallic mesh, screen or particles, in a packed or fluidized bed. In catalytic converters, frequently a washcoat is used as support of the catalytic surface. In the monolith-type automobile catalytic converters, the washcoat is made of sintered alumina

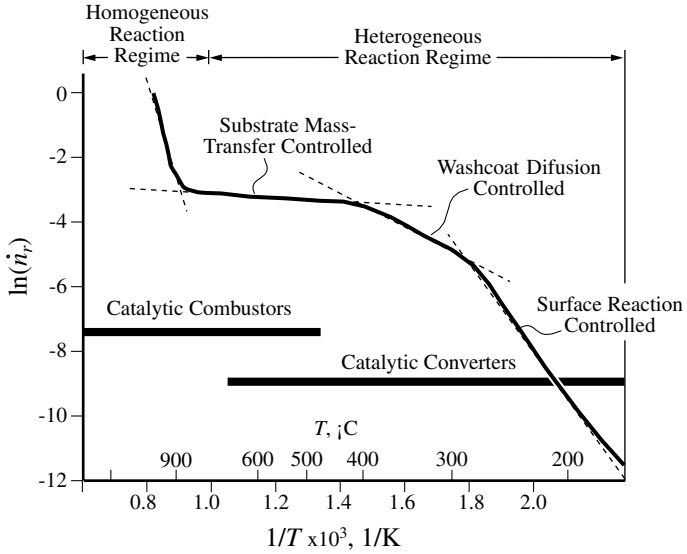

Fig. 9. Reaction rate (arbitrary units) for CO oxidation on a Pt coated, monolith-type, catalytic converter [18].

agglomerates 10–100 nm in diameter, formed by primary alumina particles which are 1–2 nm in size. The precious metal (platinum, palladium and rhodium) crystallites are spread over the surface of the alumina particles. Manufacturing techniques for supported metal catalysts include precipitation and coprecipitation, impregnation, ion-exchange and sol–gel [98–104].

The conversion efficiency of gas pollutants depends on chemical reaction and transport limitations. Fig. 9 shows the reaction rate for the CO oxidation on a Pt coated, monolith-type, catalytic converter [18]. The reaction rate is initially controlled by the chemical kinetics of the reactions. As the temperature increases, the reaction rate increases exponentially and, for intermediate temperatures, diffusion through the washcoat becomes the controlling mechanism. With a further increase in temperature, the diffusion coefficient for gases increases and surface convection mass transfer through the large channels of the monolith (the flow is usually laminar) becomes the controlling mechanism. In the steady-state operational temperature range of underfloor catalytic converters (short excursions to high temperatures are possible), the kinetics of the chemical reactions and the transport in the washcoat control the pollutant conversion.

The modeling aims at a basic understanding of the reaction and transport which would ultimately allow for the optimization of the catalytic surfaces and substrates for a given application [106]. The modeling of the catalytic particles (pellets or washcoat) requires a description of the geometry of the porous structure and its change with time, and a treatment of the surface reactions and heat and mass transfer.

The description of the geometry of the support includes the size and shape of pores, connectivity of the network of pores and geometry of the surfaces (e.g. smooth or fractal). The selectivity and activity of a catalytic surface depends on the average size, geometry and distribution of crystallites, physical interactions between the metals, composition of the support and the presence of other promoters. Electron microscopy (with atomic resolution and transmission electron microscopy) allows for the visualization of the shape, size and distribution of crystallites down to the 1 nm size range [99]. X-ray diffraction can also give average diameter and scanning tunneling microscopy can give particle shape. Different lattice planes can be exposed at the crystallite surface and they may present line and point defects. The lattice planes and defects can be highly variable, depending on the pretreatment and environmental conditions [98]. During preparation, small amounts of oxide from the support may also be transported to the crystallite surface. Techniques using high-intensity fluxes of X-ray (e.g. from synchrotron radiation sources) can provide information on metal–metal bond distance, metal coordination number, disorder of surface atoms and size and shape of supported metal clusters [98,108]. The structure may change with time as a result of chemical reaction, poisoning, or thermal stress. The catalytic surface may lose its activity due to sintering and poisoning. Sintering depends on the temperature and composition of the gas mixture. Sintering of platinum particles supported on alumina occurs by crystallite migration and coalescence by surface diffusion, duct ripening and Ostwald ripening [105]. Pt and Rh particles are more stable under reducing conditions, while Pd particles are more stable under oxidizing conditions. This makes Pd the choice for lean-burn engines allowing for the placement of the converter closer to the engine which results in a faster light-off. Poisoning, mostly sulfur and phosphorus poisoning, occurs by the deactivation of active sites and plugging of the porous structure due to the growth of solid phases.

The growth of solid phases is kinetic and transport controlled and occurs by a mechanism similar to the catalytic hydrodemetallation of crude oil process [106,107].

The surface reaction rates have been traditionally modeled following a Langmuir–Hinshelwood or Rideal–Eiley mechanism, extended to include multicomponent effects on the inhibition. The active sites are supposed to exist at a given surface concentration at the interface between the solid and gas phases, i.e. coating the solid particles. The predictions of these models are then compared to the integral conversion measurements and the reaction rate coefficients are adjusted to predict the measurements. Although these models are able to predicted steady-state results for different conditions, they do not provide an accurate description of multiple steady-states, oscillations, and chaotic behavior [98]. It has been shown that the chemical kinetics are sensitive to the geometry of the surface (exposed lattice planes, defects) and to the distribution of crystallites [98]. A more basic understanding of the surface reactions requires theoretical and surface chemistry methods [109]. The theoretical methods include Monte Carlo simulations, molecular dynamics and quantum chemistry. The surface chemistry methods include infrared, Raman and NMR spectroscopy. These allow for the observation of the structure and composition of the adsorbed species. The observations are usually made on very well defined crystals under ultrahigh vacuum conditions.

The mass transfer involves bulk and surface multicomponent diffusion. The effective diffusivity of a gas in a porous medium $\langle D_m \rangle$ depends on the geometry, the molecular diffusivity of the gas in the mixture and the pore size. Fig. 10 shows the dependency of the effective diffusivity on pore size [99] for a given molecule and temperature. The effective diffusivity becomes a strong function of pore size in the Knudsen regime (when the mean-free path of the gas molecules is of the same order of magnitude as the pore size) and drops sharply as the pore size reaches the molecule size (hindered or configurational diffusion regime [119,120]). The diffusion through the washcoat is usually modeled using continuous models. The effective diffusivity accounts for the effect of the pore structure on the diffusion of the different components. The dusty-gas model is also used. It has been shown [110–112] that bulk pressure gradients can develop inside of the porous catalyst as a result of external pressure gradients and mass diffusion induced bulk flow due to the reaction stoichiometry. In modeling diffusion using networks, it is important to reproduce the connectivity and the conductance of the individual pores, statistically, as close as possible. The pore size distribution can be obtained from sorption experiments [121], mercury porosimetry [122], and image analysis [124]. Jerauld et al. [113,114] point that there are short-range correlations between the transport properties of the pores. However, they showed that as long as the average coordination number (a measure of connectivity) and distribution of conductances of the channels is reproduced correctly, the effective transport properties calculated from a regular network (e.g. a square network) are equal to the ones exhibited by a random network. One of the network models that has been used to model random pore structures is the Swiss–Cheese model, which leads to a Voronoi tessellation that represents the porous channels [115]. The mass transport through the channels of the monolith have been modeled using surface-convection correlations, assuming either plug or Poiseuille flows and well-mixed sites (nodes). Transient effects are generally not included.

The accuracy of continuous models in describing transport and reaction in porous media has also been investigated. The questions are whether the effective diffusivity is a function of the reaction rate, if use of an effective diffusivity fails near percolation thresholds and whether it is accurate enough in modeling diffusion of molecules with diameters approaching the pore size. The continuum models agree with network results when the multiple scales are taken into account [106]. Zhang and Seaton [116] used a regular, three-dimensional network, with smooth cylindrical pores. At the pore-level, they assumed one-dimensional, steady-state diffusion-reaction with first-order reaction and well-mixed sites. Their results show that the effective diffusivity calculated in absence of reaction is equal to the one calculated with reaction, as long as there is sufficient penetration of the diffusion front into the modeled network. This is due to the fact that the continuum model fails when the length scale for the penetration is of the same order of magnitude as the pore length. The continuum model also fails near the threshold of percolation caused by pore blockage during poisoning. The correlation length (i.e. the length scale over which the fluid phase is connected) is given in Ref. [115]

$$\xi |P - P_c|^{-\nu}, \tag{22}$$

where P is the probability of a single pore being blocked, P_c the critical probability (probability at the percolation threshold)

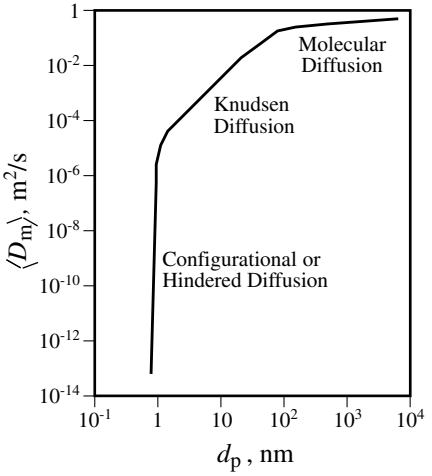

Fig. 10. Effect of pore size on the effective diffusivity [99].

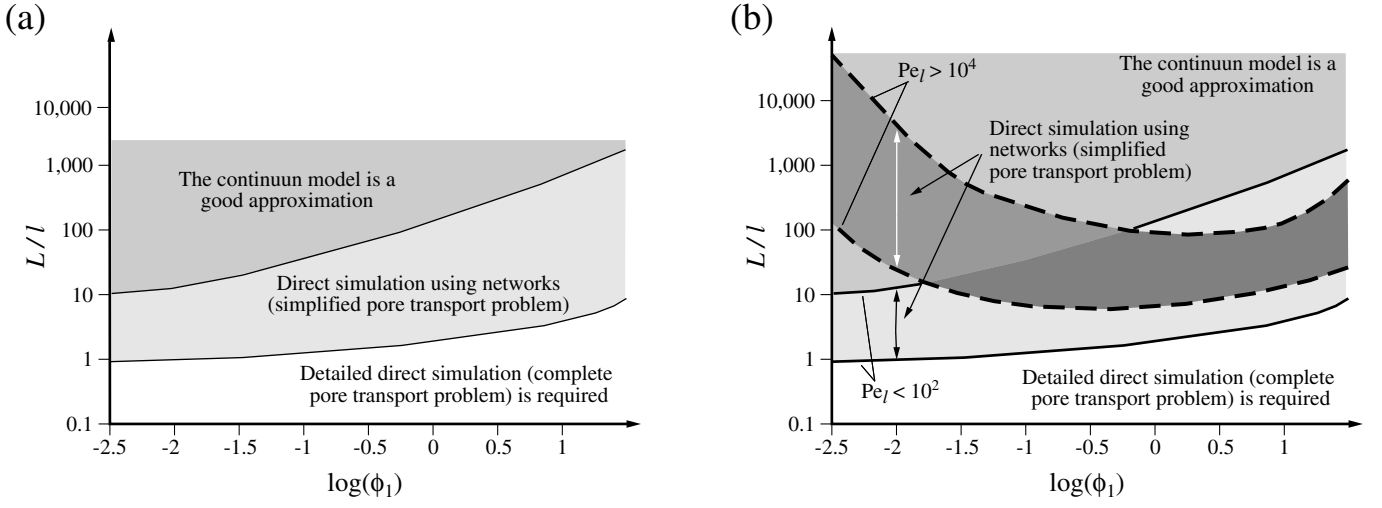

Fig. 11. Domains for the modeling of the diffusion and reaction in a porous pellet for: (a) uniform reaction rate constants; and (b) nonuniform reaction rate constants. ϕ_1 is the pore Thiele modulus and L/l is the ratio of system to pore lengths.

and ν is an exponent which depends on the dimensionality ($\nu = 0.88$ for a three-dimensional network). The correlation length tends to infinity when the percolation threshold is reached and, therefore, becomes much larger than the system length L. As the pore size reaches the size of the molecules, a threshold for percolation may also be reached. From the results of Zhang and Seaton, these trends are summarized in Fig. 11a. The Thiele modulus ϕ_l is defined as

$$\phi_l = \frac{l^2 a_1}{D^{\beta}_{i,m}} \frac{S_{\beta\sigma}}{\varepsilon_{\beta}}, \tag{23}$$

where a_1 is the reaction rate constant (in m/s) and l the pore length. For a smooth cylindrical pore with radius r_p, $S_{\beta\sigma}/\varepsilon_{\beta} = 2/r_p$.

In the model of Zhang and Seaton [116], the reaction rate constant was uniform for the network. In practice, there may be nonuniformity in reaction constants due to variations in crystallite distribution and crystallite activity (related to size, shape, surface state, poisoning, etc). These nonuniformities have their own characteristic length scales which vary from crystallite, to pore, to system size. When the nonuniformity is very pronounced, a percolation threshold may also be reached. Alvarado et al. [117] investigated the effect of a bimodal spatial nonuniformity on the reaction constant in transient diffusion and adsorption of a chemical species in a porous network. They used a two-dimensional square network of cylindrical pores with $l \gg r_p$ and assumed a pore-level one-dimensional diffusion–convection–reaction model. They concluded that for uniform reaction constants, the dispersion coefficient (which accounts for the effect of effective diffusivity and flow in the spreading of a chemical species) is not a function of reaction rate (i.e. it is purely hydrodynamic) and the effective reaction constants are equal to the pore-level ones. However, when the reaction constants are nonuniform, the dispersion coefficient becomes a function of the reaction rate when the characteristic Damköhler number (where u is the pore average velocity and $a = a_2/a_1$ the chemical equilibrium constant for an adsorption/desorption reaction)

$$Da_l = \frac{la^2 a_1}{u} \frac{S_{\beta\sigma}}{\varepsilon_{\beta}}, \tag{24}$$

is small ($Da_l \to 0$). This condition is reached, for example, when the pore-level Peclet number ($Pe_l = ul/D^{\beta}_{i,m}$) is large or when the reaction rates are small. They showed that for large Peclet numbers ($Pe_l > 10^4$), the transport and reaction is dominated by both convection and reaction. When $Pe_l \to 0$, diffusion dominates, and the reaction and transport effects are decoupled. Also, when the system size becomes very large ($L \gg l$) the dispersion coefficient approaches a purely hydrodynamic behavior. The Damköhler number is proportional to the ratio of the Thiele modulus and Peclet number, $Da_l \sim \phi_l/Pe_l$. Thus, in the presence of flow, a small Thiele modulus may also require detailed simulation, as summarized in Fig. 11b. A pore with a fractal surface (large $S_{\beta\sigma}$) would increase the Thiele modulus and a surface effectiveness, which accounts for the accessibility of the surface to the gas molecules, can be defined. Coppens and Froment [118] show that the surface effectiveness of the fractal pore is smaller than the one for a circular pore with the same length. They also conclude that it is usually impossible to construct a smooth cylindrical pore which results in the same flux and end concentrations of a reactant species as the pore with a fractal surface.

The role of diffusion within the washcoat in the chemical conversion rates is not yet fully understood. The choice of agglomerate size used for the washcoat depends on design parameters such as activity of the washcoat, adherence to the substrate, mechanical strength under thermal loading, and other durability and reliability requirements. In most cases, a unity washcoat effectiveness is assumed and the precious metal loading is adjusted to predict the overall conversion rates for different operating conditions. Although the current generation of catalytic converters is overdesigned from a mass-transport perspective, the continuous decrease in the tolerable levels of emissions leads to the necessity of a closer examination of the effect of washcoat diffusion on the conversion of gas pollutants at low pollutant concentrations (to find ways of increasing the washcoat effectiveness for a given precious metal loading). This requires a detailed modeling of the reaction and transport in the washcoat. Also, the development of fast and accurate design tools for engineering treatment of washcoat diffusion that can be easily incorporated into existing design packages is necessary. Fig. 12 presents a summary of the modeling and experiments for the design and optimization of catalytic converters, showing the many length scales in which optimization is possible.

In the next two sections, systems for which chemical nonequilibrium is a result of intrinsic characteristics are presented. The control of geometry and of process aims at increasing combustion rates.

4.3. Solid pyrolysis

Pyrolysis occurs as a result of the thermal degradation of a solid fuel. Wood burning for energy generation [53,54], waste incineration [57,97], and fire propagation [55,56] are examples of processes involving pyrolysis. Fig. 13 illustrates the coexisting gas- and solid-phase reactions in a combustible porous medium. The porous medium consists of a packed bed of randomly arranged spherical wood particles. The upward flow of the air against the gravitational field is in the opposite direction to that of the combustion wave. This is called reverse smoldering. The solid undergoes pyrolysis generating a volatile fuel to react with the oxygen available in the gas phase. Heterogeneous reactions can take place concurrently with the gas-phase reactions (homogeneous). The extent of the surface reactions depends on the rate of oxygen diffusion to the surface of the char produced subsequent to the pyrolysis. Four distinct regimes

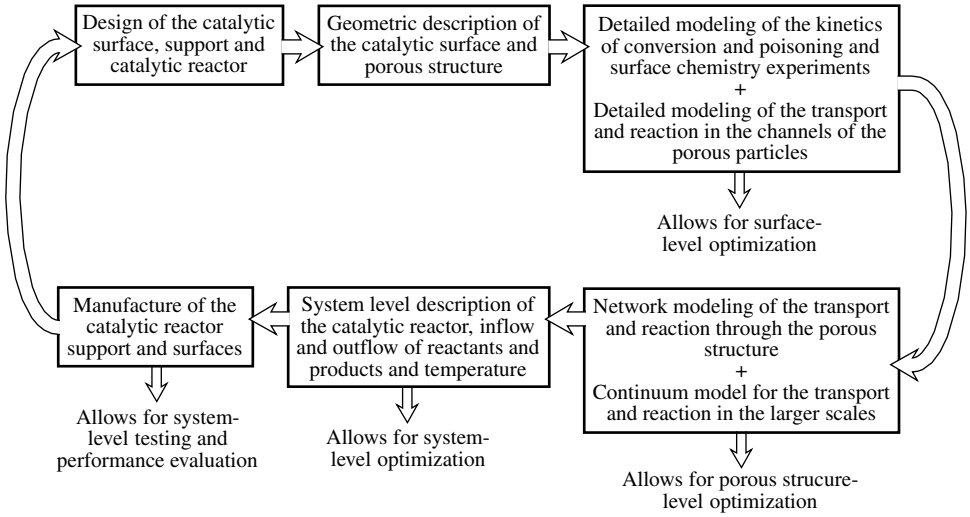

Fig. 12. Design and optimization of catalytic converters.

exist: heating and drying of the wood particles; pyrolysis; char oxidation; and gas-phase reaction regimes (flaming). For a given fuel bed porosity and particle size, the intensity, relative position, and width of the reaction zones are not known a priori and can vary greatly depending on the flow rate of the incoming gas, the initial concentration of the oxygen in the flow, and the chemical kinetics and thermal effects.

The pyrolytic reaction is initiated ahead of the char oxidation zone, generating the volatile fuel to burn in the gas phase further downstream. The pyrolysis takes place at a much faster rate than the char oxidation, being, usually, nearly complete at the start of the char oxidation. The pyrolysis zone may, however, extend over the char oxidation zone. In this case, while the char oxidation is taking place at the surface, the pyrolysis may still continue in the interior of the particle. The flow rate of the incoming air has negligible effect on the thickness of the pyrolysis zone. In contrast to the char oxidation, the pyrolysis is independent of the oxygen concentration in the gas and its availability. In the presence of nitrogen, it depends only on the local solid temperature. For wood particles, pyrolysis temperatures are typically from 625 to 635 K. It is interesting to note that since the temperature gradient within the pyrolysis zone does not change significantly with variations in the incoming gas flow rate, the concentration of the volatiles in the solid phase also remains unaffected by the gas pore velocity.

The solid surface can also suppress the gas-phase reactions due to a third body recombination of the free radicals, which participate in the gas-phase combustion. Thus, in a packed bed the gas-phase reactions can be inhibited because of the large specific surface area of the solid. In this situation, the smoldering is sustained by the char oxidation reactions.

The char oxidation reactions are kinetically controlled at

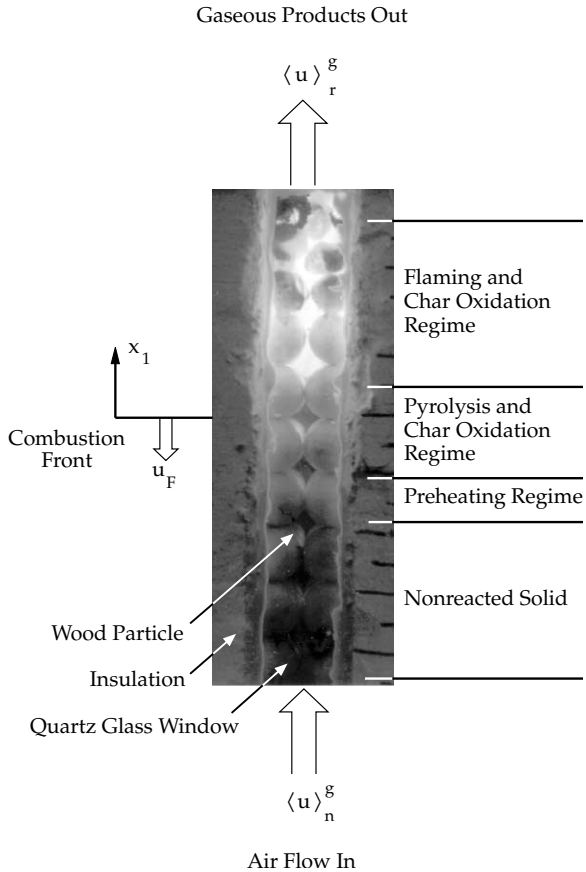

Fig. 13. Rendering of the coexisting gas- and solid-phase reactions in a combustible porous medium [54].

low temperatures. At high temperatures, the rate-controlling path is the diffusion rate of oxygen from the bulk gas to the surface of the solid particle, i.e. it becomes mass transfer controlled. Mass diffusion to the particle surface is usually modeled using a solid–gas mass transfer coefficient. The overall local volume-averaged heterogeneous reaction rate is given by an Arrhenius expression [54,58].

The condition of local thermal equilibrium between the gas and solid phases breaks down in the reaction zone. The transfer of some of the heat through the solid to the reactants in the gas phase causes a temperature increase in the flame (and in turn, heat transfer to the solid). The gas phase thus exhibits a superadiabatic temperature. The excess temperature and the gas- and solid-phase temperatures throughout the combustion wave increase as the incoming air flow rate increases.

The combustion rate can be increased by reducing the thermal nonequilibrium. This can be done by decreasing the particle size. Smaller particle size increases the optical thickness and decreases the effective thermal conductivity. A maximum combustion rate can be achieved for an optimum particle size. The use of a gas fuel to increase the rate of pyrolysis can be used for low calorific fuels.

4.4. Powder combustion

In contrast to the gas–solid reactions in smoldering, the reactions between two components in the form of particles may be controlled by the interparticle rate of transfer of reactants. In the propagation mode of combustion synthesis (or SHS, self-propagating, high-temperature synthesis) [62–69], a compacted-powder specimen is ignited at one end and a combustion wave travels through it converting the reactants to products. This method has been used to produce ceramics, intermetallics, cermets, composites, functionally gradient materials, thin coatings, and to join materials. It has been observed experimentally that complete conversion may not occur and the maximum temperature in the combustion region may be substantially below the adiabatic equilibrium temperature [63]. In gasless combustion synthesis (i.e. combustion with no participation or generation of a gas phase) of intermetallics, this lack of complete reaction has been related to the heterogeneous nature of the polysized, multicomponent particle mixture (affecting the heat transfer, diffusion, and phase transformation) [67,68].

The modeling of gasless combustion synthesis requires descriptions at the specimen and particle scales, as shown in Fig. 14. At the specimen scale, the heat transfer, the volumetric heat generation, and the peripheral heat losses, determine the axial temperature distribution. The volumetric heat generation depends on the particle-level mass transfer, reaction rates, and phase transformations. The kinetics of these intraparticle processes depends on the temperature and chemical composition, which is affected by species diffusion and by the interparticle availability of reactants. This local (i.e. interparticle) stoichiometry may differ from the specimen-level average stoichiometry because of the inherent heterogeneity of the medium which increases in the presence of a particle size distribution. The interactions between specimen-level and particle-level processes determine the final microstructure, including the composition and distribution of product phases and the amount of reactants remaining, and the mechanical and morphological transformations during the combustion synthesis, including the formation and destruction of porosity (i.e. consolidation), the mechanical stability of the compacts during reaction, and the products mechanical and metallographic properties. The modeling of the mechanical transformations requires thermomechanical descriptions. A phase field formulation can be potentially used to model the particles transformations and motion [127,128].

Armstrong [69] used a thin-flame asymptotic method to solve for the propagation speed of thin laminae stacked parallel and perpendicular to the propagation front and randomly arranged. His solution for the propagation speed is

$$u_F^2 = \frac{cD_o \dfrac{R_g T_r}{\Delta E_d}\alpha}{\delta_d^2 \dfrac{T_r - T_o}{T_r}} \exp\left(\frac{-\Delta E_d}{R_g T_r}\right) \tag{25}$$

where T_r is the reaction (maximum) temperature, T_i the initial temperature, D_o the preexponential factor for the diffusion coefficient of one reactant into the particle of the other reactant, δ_d is the diffusion length associated with the laminae thickness (i.e. particle size) and c is a constant ($c = 3$ for laminae stacked parallel to the flame propagation direction and $c = 12$ for the random arrangement).

Comparing this model with a premixed-type model [63] the effective preexponential factor of the premixed-type model is given by

$$A_o = \frac{c}{f(n)} \frac{D_o}{\delta_d^2} \tag{26}$$

where $f(n)$ is a function of the order of the reaction n ($f(n) = 2$ for $n = 0$, $f(n) = 1.1$ for $n = 1$ and $f(n) = 0.73$ for $n = 2$).).

Assuming that the diffusion length δ_d is of the order of $r_p \sim 10^{-6}$ m, and using a representative value of $D_o \sim 10^{-4}$ m^2/s, the Armstrong scale gives $A_o \sim 10^7$ 1/s. The activation energy is of the order of $\Delta E_d \sim 10^8$ J/kmol. However, we note that this effective preexponential factor does not remain constant along the reaction, because the diffusion length δ_d is a function of time [68].

The powders commonly used present a nonuniform distribution of particle size and shape. This nonuniform particle-size distribution has two effects. First, since the chemical reaction is diffusion controlled, particles of different sizes experience different reaction rates and temperature evolution, thus, influencing the specimen-level temperature distribution and propagation speed. This effect depends primarily on the average particle size. Second, a nonuniform distribution of reactants changes the local stoichiometry and the

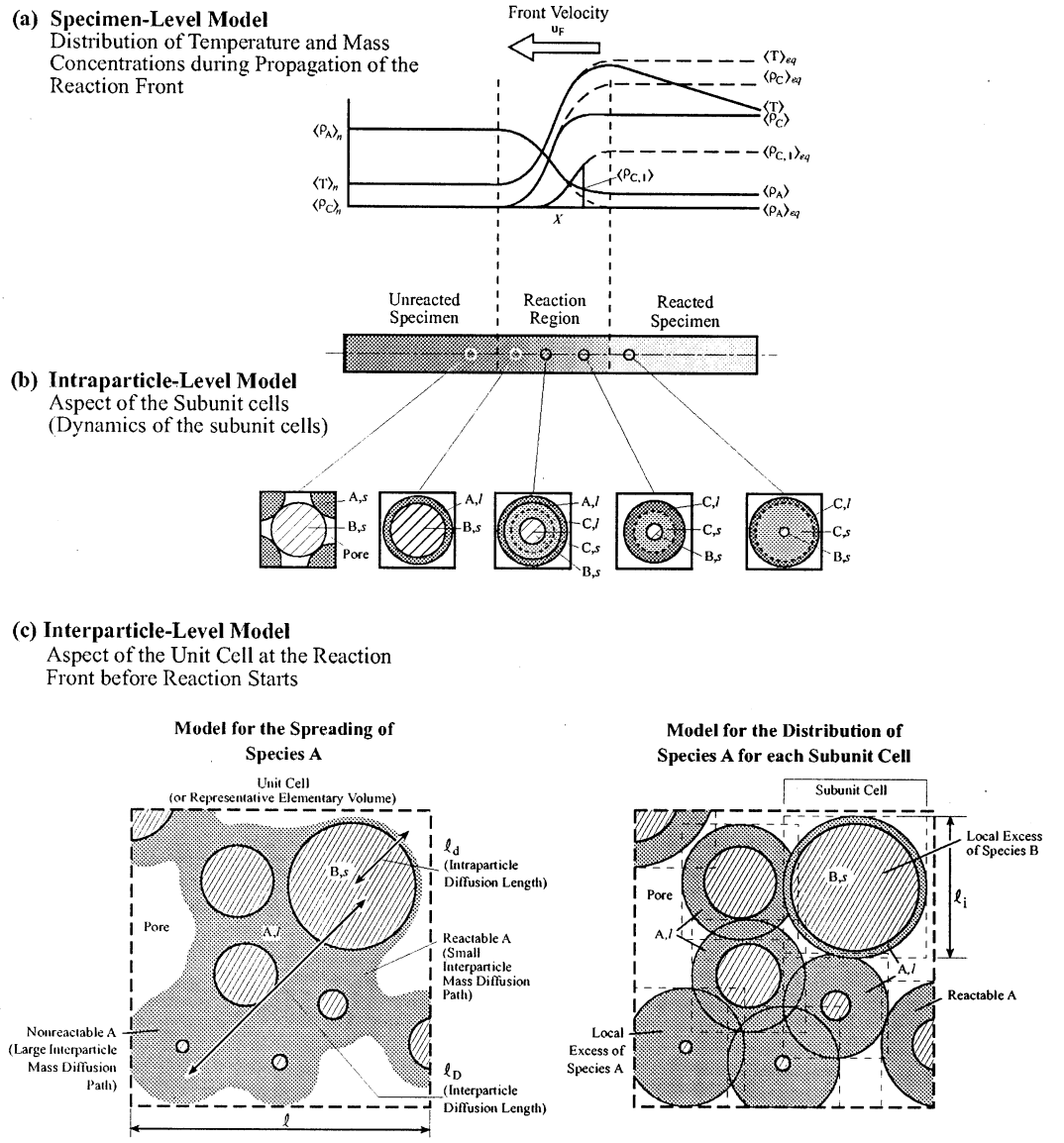

Fig. 14. (a) Rendering of the specimen-level temperature and mass concentration distributions. (b) Variations in the structure of a particle along the specimen during reaction (using a shrinking-core model). (c) Modeling of the nonuniform particle-size distribution, showing the fraction of species A that may not reach the species B particles [67].

distance separating the melt-rich regions from the melt-lean regions may be large. The peripheral heat losses would then prevent the timely migration of the melted reactant. This effect depends on the shape of the particle size distribution, especially the standard deviation. As a consequence, among other chemical and phase equilibrium requirements, a uniform particle size distribution is needed for complete conversion and a small average particle size is needed for propagation. These would require screening of the powders which would then increase the production cost.

5. Summary

The recent advances in modeling and understanding of combustion in porous media and the recent experimental findings have allowed for the design of new combustion processes and systems, such as, catalytic reactors and converters, direct energy and gas conversion devices and systems, chemical sensors and materials synthesis processes. These novel materials, devices, equipment and synthesis processes have advanced the understanding and

modeling of reaction in porous media to new levels, requiring the use of multiple disciplines and experimental and theoretical tools. Advances in gas-phase and surface chemistry, solid-state and condensed-phase physics, transport in disordered structures, mathematical and numerical methods to analyze continuum and statistical models have allowed for deeper investigations into the kinetics of reactions, thermodynamic and transport properties and their interaction with the transport processes. The improvement of the current and the design of yet newer and more innovative systems require further investigations into the mechanisms of heat and mass transport and reaction and their interactions with the structure within porous media.

Superadiabatic combustion and local chemical nonequilibrium, including optimal fuel distribution, are very promising for innovative new combustion systems. The conduction and radiation along the porous media may be optimized by the proper choice of the material and structure, thus increasing the superadiabatic effect. Optimal fuel distribution is achieved by the proper design of the porous structure to attend the thermal load. The output of the radiant burners may be improved by a proper choice of the material and geometry near the surface. Thermal regeneration also depends on the choice of the material and geometry. High conductivity, high volumetric heat capacity and low effective thermal conductivity materials and structures are desirable for optimal heat storage and recirculation.

Surface science of adsorption, diffusion, and reaction need to be better understood for optimal design and innovative applications of catalytic combustion. The increase in the conversion rate of trace pollutants, depends on the optimization of the porous structure and catalytic site distribution for large surface area and low resistance to mass diffusion. Bimodal pore-size distributions with axial and transversal nonuniform crystallite distribution may lead to an optimum performance. Catalytic surfaces and supports which are resistant to poisons and active in oxidizing exhaust conditions (e.g. the emission from diesel and lean-burn engines) need to be developed, especially NO_x catalysts. High-temperature catalytic surfaces for complete and partial combustion of methane are also needed. The understanding and modeling of chemical nonequilibrium in washcoats (and supports) is required for the development of these applications. New trends in the modeling of diffusion within porous structures is addressed in a recent review [132].

The understanding of the solid pyrolysis allows for control and prevention of fire and a more efficient use of solid fuels. The ability to suppress or augment the pyrolysis rate leads to a better control of the combustion.

The control of the nonuniform distribution of reactants in combustion synthesis and a better understanding of the mechanisms of dynamic phase nucleation and growth are needed for a better control of the conversion rates. This allows for attaining complete conversion, or producing a functionally gradient material. Also, the potential of the method as a near net-shape manufacturing strategy has not yet been exhausted.

References

[1] Takeno T, Sato K. Combust Sci Technol 1979;20:73–84.
[2] Yoshizawa Y, Kiyoshi S, Echigo R. Int J Heat Mass Transfer 1988;31:311–9.
[3] Sathe SB, Peck RE, Tong TW. Int J Heat Mass Transfer 1990;33:1331–8.
[4] Echigo R. Radiation enhanced/controlled phenomena of heat and mass transfer in porous media. Proceedings of the First ASME/JSME Joint Thermal Engineering Conference, vol. 4, 1991. p. 21–32.
[5] Hsu PF, Howell JR. Exp Heat Transfer 1993;5:293–313.
[6] Hsu P, Matthews RD. Combust Flame 1993;93:457–66.
[7] Kanna R, Goel JL. Ellzey. Combust Sci Technol 1994;99:133–42.
[8] Sahraoui M, Kaviany M. Int J Heat Mass Transfer 1994;37:2817–34.
[9] Tong TW, Li W. J Quant Spectrosc Radiat Transfer 1995;53:235–48.
[10] Howell JR, Hall MJ, Ellzey JL. Prog Energy Combust Sci 1996;22:121–45.
[11] Rumminger MD, Dibble RW, Heberle NH, Crosley DR. Gas temperature above a porous radiant burner: comparison of measurements and model predictions. Proceedings of the 26th Symposium (International) on Combustion/The Combustion Institute, 1996. p. 1755–62.
[12] Hackert CL, Ellzey JL, Ezekoye OA. Combust Flame 1999;116:177–91.
[13] Malico I, Pereira JCF. Sensitivity study on the influence of radiative properties in porous media combustion. Proceedings of the V International Conference on Technologies for a Clean Air Environment, Lisbon, 1999. p. 555–62.
[14] Brenner G, Pickenäcker K, Pickenäcker O, Trimis D, Wawrzinek K, Weber T. Stabilised combustion and heat transfer in porous inert media — an experimental and numerical study. Proceedings of the V International Conference on Technologies for a Clean Air Environment, Lisbon. 1999, p. 525–31.
[15] Kesting A, Pickenäcker O, Pickenäcker K, Trimis D. Application of the porous burner technology in energy and heat engineering. Proceedings of the V International Conference on Technologies for a Clean Air Environment, Lisbon, 1999.
[16] Malico I, Pereira JCF. J Porous Media 1999;2:153–62.
[17] Saracco G, Cerri I, Specchia V, Accornero R. Chem Engng Sci 1999;54:3599–608.
[18] Koberstein E, Wannemacher G. Catalysis and automotive pollution control, SAE, 1987. p. 155–72.
[19] Beeckman JW, Hegedus LL. Ind Engng Chem Res 1991;30:969–78.
[20] Tamaru K, Mills GA. Catal Today 1994;22:349–60.
[21] Armor JN. Catal Today 1995;26:99–105.
[22] Pfefferle WC, Pfefferle LD. Prog Energy Combust Sci 1986;12:25–41.
[23] Pfefferle WC, Pfefferle LD. Catal Rev — Sci Engng 1987;29:219–67.
[24] Barresi AA, Hung SL, Pfefferle LD. Chem Engng J 1992;50:123–31.
[25] Ikeda H, Libby PA, Willians FA. Combust Flame 1993;93:138–48.
[26] Markatou P, Pfefferle LD, Smooke MD. Combust Flame 1993;93:185–201.
[27] Pfefferle LD. Catal Today 1995;26:255–65.

[28] Dalla Betta RA, Schlatter JC, Yee DK, Loffler DG, Shoji T. Catal Today 1995;26:329–35.
[29] Arai H, Fukuzawa H. Catal Today 1995;26:217–21.
[30] Maruko S, Naoi T, Onedera M. Catal Today 1995;26:309–17.
[31] Eguchi K, Arai H. Catal Today 1996;29:379–86.
[32] Jones R. Surf Coat Technol 1997;95–96:118–22.
[33] Niehorster C, Arends G, Schreiber M. Combust Flame 1997;110:140–51.
[34] Hickman DA, Schmidt LD. AIChE J 1993;39:1164–77.
[35] Schmidt LD, Huff M, Bharadwaj SS. Chem Engng Sci 1994;49:3981–94.
[36] Bharadwaj SS, Schmidt LD. Fuel Process Technol 1995;42:109–27.
[37] Ziauddin M, Balakrishna A, Vlachos DG, Schmidt LD. Combust Flame 1997;110:377–91.
[38] Ferrenberg A. SAE Trans, SAE 900911, 1990.
[39] Ferrenberg A. AIAA J, AIAA 90-2510, 1990.
[40] Ferrenberg A. SAE Trans, SAE 940946, 1994.
[41] Hanamura K, Bohda K, Miyairi Y. Energy Convers Mgmt 1997;38:1259–66.
[42] Fateev GA, Rabinovich OS. Int J Hydrogen Energy 1997;27:915–24.
[43] Park C-W, Kaviany M. Combustion thermoelectric tube. Proceedings of the 1999 National Heat Transfer Conference, Albuquerque, New Mexico, 1999.
[44] Park C-W, Kaviany M. J Heat Transfer. ASME J Heat Transfer 2000;122:721–90.
[45] Hanamura K, Akagi K, Koyanagi K. Autothermic reforming by reciprocating-flow super-adiabatic combustion in porous media. Proceedings of the Fifth ASME/JSME Joint Thermal Engineering Conference, San Diego, California, 1999. p. 1–6.
[46] Park C-W, Kaviany M. Optimization of high-temperature radiant burner. Report to Air Liquide, CRCD, Joay-en-Josas, France, 1999.
[47] Kesting A, Pickenäcker O, Trimis D, Durst F. Development of a radiation burner for methane and pure oxygen using the porous burner technology. Proceedings of the V International Conference on Technologies for a Clean Air Environment, Lisbon, 1999.
[48] Farrauto RJ. React Kinet Catal Lett 1997;60:233–41.
[49] MacIntosh AC, Bains M, Crocombe W, Griffiths JF. Combust Flame 1994;99:541–50.
[50] Kaplan M, Hall MJ. Exp Thermal Fluid Sci 1995;11:13–20.
[51] Martynenko VV, Echigo R, Yoshida M. Int J Heat Mass Transfer 1998;41:117–26.
[52] Kanury AM, Blackshear Jr. PL. Combust Sci Technol 1970;1:339–55.
[53] Di C. Blasi. Combust Sci Technol 1993;90:315–40.
[54] Fatehi M, Kaviany M. Combust Flame 1994;99:1–17.
[55] Schult DA, Matkowski BJ, Volpert A, Fernandez-Pello AC. Combust Flame 1996;104:1–26.
[56] Torero JL, Fernandez-Pello AC, Kitano M. Combust Sci Technol 1993;91:95–117.
[57] Brereton C. Resour Conserv Recycl 1996;16:227–64.
[58] Fatehi M, Kaviany M. Int J Heat Mass Transfer 1997;40:2607–20.
[59] Garner CP, Dent JC. Trans SAE, Paper, S.A.E., No. 880007, 1988.
[60] Noirot R, Gilot P, Gadiou R, Prado G. Combust Sci Technol 1994;95:139–60.
[61] Koltsakis GC, Stamelos AM. Ind Engng Chem Res 1996;35:2–13.
[62] Munir ZA. Ceram Bull 1988;67:342–9.
[63] Merzhanov AG. Self-propagating high-temperature synthesis: twenty years of search and findings. In: Munir ZA, Holt JB, editors. Combustion and plasma synthesis of high temperature materials. New York: VCH; 1990 [chap. 1].
[64] Varma A, Rogachev AS, Mukasyan AS, Hwang S. Adv Chem Engng 1998;24:79–226.
[65] Brezinski K. Gas-phase combustion synthesis of materials. Proceedings of the 26th Symposium (International) on Combustion/The Combustion Institute, 1996. p. 1805–16.
[66] Wooldridge M. Prog Energy Combust Sci 1998;24:63–87.
[67] Oliveira AAM, Kaviany M. Int J Heat Mass Transfer 1999;42:1059–73.
[68] Oliveira AAM, Kaviany M. Int J Heat Mass Transfer 1999;42:1075–95.
[69] Armstrong R. Combust Sci Techol 1990;71:155–74.
[70] Whitaker S. Simultaneous heat, mass, and momentum transfer in a porous media: a theory of drying. In: Hartnett JP, Irvine I, editors. Advances in heat transfer, 7. New York: Academic Press; 1977. p. 119–203.
[71] Whitaker S. Chem Engng Sci 1986;41:3015–22.
[72] Quintard M, Whitaker S. Transport Porous Media 1988;3:357–413.
[73] Prat M. Transport Porous Media 1989;4:259–80.
[74] Whitaker S. Heat transfer in catalytic packed bed reactors. In: Cheremisinoff NP, editor. Handbook of heat and mass transfer. Gulf, Matawan, New Jersey, 1989.
[75] Plumb OA, Whitaker S. Diffusion, adsorption and dispersion in porous media: small-scale averaging and local volume averaging. In: Cushman JH, editor. Hierarchy of scales in subsurface transport. London: Academic Press; 1990.
[76] Quintard M, Whitaker S. Transport Porous Media 1990;5:341–79.
[77] Whitaker S. Ind Engng Chem Res 1991;30:983–97.
[78] Quintard M, Whitaker S. One- and two-equation models for transient diffusion processes in two-phase systems. In: Hartnett JP, Irvine TF, editors. Advances in heat transfer, 23. New York: Academic Press; 1993. p. 369–464.
[79] Quintard M, Whitaker S. Chem Engng Sci 1993;48:2537–64.
[80] Quintard M, Whitaker S. Transport Porous Media 1994;14:163–77.
[81] Quintard M, Whitaker S. Transport Porous Media 1994;14:179–206.
[82] Quintard M, Kaviany M, Whitaker S. Adv Water Resour 1997;20:77–94.
[83] Kaviany M. Principles of heat transfer in porous media. Corrected 2nd ed. Berlin: Springer; 1999.
[84] Vortmeyer D. Radiation in packed solids. Proceedings of the Sixth International Heat Transfer Conference, Toronto, Canada, vol. 6, 1978. p. 525–39.
[85] Tien CL, Drolen BL. Thermal radiation in particulate media with dependent and independent scattering. Annual review of numerical fluid mechanics and heat transfer, Washington: Hemisphere; 1987. p. 1–32.
[86] Viskanta R, Menguç MP. Appl Mech Rev 1989;42:241–59.
[87] Tong TW, Sathe SB, Peck RE. Int J Heat Mass Transfer 1990;33:1339.
[88] Singh BP, Kaviany M. Radiation in porous media. In:

Hartnett JP, Irvine TF, editors. Advances in heat transfer, 23. New York: Academic Press; 1993. p. 369–464.
[89] Hendricks TJ, Howell JR. J Heat Transfer 1996;118:79–87.
[90] Doermann D, Sacadura JF. J Heat Transfer 1996;118:88–93.
[91] Fu X, Viskanta R, Gore JP. Int Commun Heat Mass Transfer 1997;24:1069–82.
[92] Furmanski P, Wisniewski S, Banaszek J. Analysis of nonlocal character of radiation heat transfer in thermal insulations. Proceedings of the 11th International Heat Transfer Conference, Kyongiu, Korea, vol. 7, 1998. p. 379–84.
[93] Kamiuto K, Matsushita T. High-temperature radiative properties of open-cellular porous materials. Proceedings of the 11th International Heat Transfer Conference, Kyongiu, Korea, vol. 7, 1998. p. 385–90.
[94] Zhdanov S, Kennedy LA, Koester G. Combust Flame 1995;100:221–31.
[95] Aldushin AP, Rumanov IE, Matkowsky BJ. Combust Flame 1999;118:76–90.
[96] Mohamad AA, Ramadhyani S, Viskanta R. Int J Heat Mass Transfer 1994;37:1181–91.
[97] Penner SS, Berlad AL. Energy 1995;20:311–24.
[98] Bell A. Chem Engng Sci 1990;45:2013–26.
[99] Gates BC. Catalytic chemistry. New York: Wiley; 1992.
[100] Bethke KA, Kung MC, Yang B, Shah M, Alt D, Li C, Kung HH. Catal Today 1995;26:169–83.
[101] Walker AP. Catal Today 1995;26:107–28.
[102] Masel RI. Principles of adsorption and reaction on solid surfaces. New York: Wiley; 1996.
[103] Gilot P, Guyon M, Stanmore BR. Fuel 1997;76:507–15.
[104] Gonzales RD, Lopez T, Gomez R. Catal Today 1997;35:293–317.
[105] Chen JJ, Ruckenstein J. J Catal 1981;69:254.
[106] Keil FJ, Rieckmann C. Chem Engng Sci 1994;49:4811–22.
[107] Arbabi S, Sahimi M. Chem Engng Sci 1991;46:1739–47.
[108] Sinfeld JH, Via GH, Lytle FW. Catal Rev — Sci Engng 1984;26:81.
[109] Keil FJ. Chem Engng Sci 1996;51:1543–67.
[110] Nan HS, Dias MM, Rodrigues AE. Chem Engng J 1995;57:101–14.
[111] Arnost D, Schneider P. Chem Engng J 1995;57:91–99.
[112] Veldsink JW, Van Damme RMJ, Versteeg GF, Swaaij WPM. Chem Engng J 1995;57:115–25.
[113] Jerauld GR, Hatfield JC, Scriven LE, Davis HT. J Phys C 1984;17:1519–29.
[114] Jerauld GR, Scriven LE, Davis HT. J Phys C 1984;17:3429–44.
[115] Sahimi M. Phys Rep 1998;306:213–395.
[116] Zhang L, Seaton NA. Chem Engng J 1994;49:41–50.
[117] Alvarado V, Davis HT, Scriven LE. Chem Engng Sci 1997;52:2865–81.
[118] Coppens M-O, Froment GF. Chem Engng Sci 1995;50:1027–39.
[119] Conner WC, Bennet CO. J Chem Soc, Faraday Trans 1993;89:4109–14.
[120] Limbach KW, Wei J. AIChE J 1990;36:242–8.
[121] Seaton NA. Chem Engng J 1991;46:1895–909.
[122] Portsmouth RL, Gladden LF. Chem Engng J 1991;46:3023–36.
[123] Bird RB, Stewart WE, Lightfoot EN. Transport phenomena. New York: Wiley; 1960.
[124] Phillipi PC, Souza HA. Int J Multiphase Flow 1995;21:667–91.
[125] Borman GL, Ragland KW. Combustion engineering. New York: McGraw-Hill; 1998.
[126] Griffiths JF. Prog Energy Combust Sci 1995;21:25–107.
[127] Cahn JW, Fife P, Penrose O. Acta Mater 1997;45:4397–413.
[128] Steinbach I, Pezzola F, Nestler B, Seeßelberg M, Prieler R, Schmitz GJ. Physica D 1996;94:135–47.
[129] Weisz PB. CHEMTEC 1973:498–505.
[130] Higler A, Krishna R, Taylor R. Ind Engng Chem Res 2000;39:1596–607.
[131] Baur R, Higler AP, Taylor R, Krishna R. Chem Engng J 2000;76:33–47.
[132] Keil FJ, Krishna R, Coppens MO. Rev Chem Engng 2000;16:71–197.
[133] Gray WG. Chem Engng Sci 1975;30:229–33.